Department of Precision and Microsystems Engineering

Design of a Vibration Energy Harvester based on Coupled Oscillators

PAULUS SCHAAP

Report no	: 2019.023
Coach	: Dr. F. Alijani, T.W.A. Blad MSc, M.P. Lustig MSc
Professor	: Prof. dr. P.G. Steeneken
Specialisation	: Dynamics of Micro and Nanosystems
Type of report	: Master thesis
Date	: July 31, 2019

TU Delft Delft University of Technology

Design of a Vibration Energy Harvester based on Coupled Oscillators

by

P. Schaap

to obtain the degree of Master of Science
at the Delft University of Technology,
to be defended publicly on Wednesday July 31, 2019 at 11:15 AM.

Student number:	4252136	
Project duration:	March 1, 2018 – July 31, 2019	
Thesis committee:	Dr. ir. F. Alijani,	TU Delft, DMN, chair, supervisor
	Prof. dr. ir. P. G. Steeneken,	TU Delft, DMN, head of department
	Ir. J. W. Spronck,	TU Delft, MSD, external examiner
	Ir. T. W. A. Blad,	TU Delft, supervisor
	Ir. M. P. Lustig	Flexous Mechanisms, company supervisor

This thesis is confidential and cannot be made public until July 11, 2024.

An electronic version of this thesis is available at `http://repository.tudelft.nl/`.

TU Delft

Preface

This work is the final part of my study at Delft University of Technology. After having taken many courses at university, it was time to work on my very own project and contribute to science. The path that led to this final work that lies before you has not always been easy, but I have learnt a lot along the way. I am grateful that I have been able to follow education of this quality having gained these experiences.
From this place I want to thank everyone that helped me realize this project. I am grateful to Farbod Alijani and Thijs Blad for their guidance, support and knowledge from university's side. I want to express my gratitude towards Maarten Lustig for his supervision and expertise from the side of the company, as well as the other company members, who were always willing to help me. I want to thank Pieter van Pelt for our discussions and advice regarding this project. Lastly, I would like to thank friends and family that supported me and helped me during this project.

P. Schaap
Delft, July 2019

Summary

Vibration energy harvesting is the solution for powering on-road sensor measurements. Various techniques to harvest the most energy from a certain application are found in literature. An electromagnetic energy harvester was found to be the best option for transport applications.
In this work, the potential benefits of a coupled oscillator electromagnetic vibration energy harvester compared to a single degree of freedom vibration energy harvester is explored. This comparison is made based on the steady-state power output when the harvester is excited at its eigenfrequencies. The harvester concepts are compared based on two cases: one where two frequencies are continuously present, and one where two frequencies are alternately present. These cases are derived from on-road container transport measurements.
A single degree of freedom and an array of two single degree of freedom harvesters are used as a benchmark. Three configurations of the coupled oscillator harvester concept are presented, which have been optimized with respect to the magnitude of the electromagnetic damping and the ratio between the two masses.
It was found that a coupled harvester with two electromagnetic dampers performs as good as an array of two single degree of freedom harvesters. When using the same proof mass for all concepts, a coupled oscillator harvester with only one electromagnetic damper generates less power than one with two dampers.
A prototype has been built to validate the simulations. Good correspondence between simulations and experiments was found, both in terms of output power and optimum electromagnetic damping.

Contents

1 Introduction

This work arose from the question which type of vibration energy harvester performs the best in transportation sector applications. First the need for vibration energy harvesting and a state of the art overview is provided in a literature survey in part I. This literature review also contains an overview of different vibration energy harvesting techniques, and ends with the suggestion to do research into multimodal energy harvesting. Part II consists of a paper and forms the main part of this work. In this part the method to compare different coupled oscillator harvesters with a single degree of freedom vibration energy harvester is described, and results are provided. The fabrication and testing of the prototype is also described here. This part ends with a discussion of the results and method used, after which conclusions and recommendations are given. As the paper tries to give a brief overview of the performed work, longer procedures and calculations are added in appendixes in part III. These appendices give a more thorough understanding of the used method and found results as described in the paper in part II.

I

Literature review

Vibration Energy Harvesting in the Transportation Sector

A Literature Review

by

P. Schaap

in partial fulfilment of the requirements for the degree of Master of Science
at the Delft University of Technology.

Student number: 4252136

Under supervision of Dr. F. Alijani (TU Delft), T.W.A. Blad MSc (TU Delft), M.L. Lustig MSc (Flexous Mechanisms)

Cover image: Kinergizer.com

Contents

1

Introduction

This literature review is part of the graduation project of the author, which has been performed at Kinergizer B.V., Delft, The Netherlands. In appendix A a work flow diagram of both the literature survey and thesis project of the author is shown. In this reports steps 1 till 6 will be taken in order to find a research gap and come up with a research question.
In this introduction, first the demand for vibration energy harvesters in the transportation sector will be discussed. After that, the goal of this literature research will be formulated, and the structure of this report will be outlined.

1.1. Market demand

There currently is a growing demand for wireless sensors in the transportation industry [59, Ch.18]. Retailers not only want to track goods to and from their worldwide suppliers, but also want to monitor parameters like temperature or acceleration for cooled and fragile products respectively. Other applications may be health monitoring of hard to reach parts in these transportation vehicles.
Most often there is no power source available at the location where a wireless sensor device is to be installed: freight train wagons are often not equipped with electric cabling, and also in lorries or on boats direct access to a power outlet is often not available. Powering these devices wireless is the most apparent option, and using batteries sounds quite obvious. Using batteries has a few drawbacks however. Firstly, their energy capacity is limited, which may result in the battery being empty before the train or boat reaches its destination. Secondly, batteries function less at low temperatures [63], which makes it harder to power devices in colder climates. Besides that, batteries are polluting to the environment once they have to be dismantled after being used, as they contain various chemical components. Lastly, replacing empty batteries will become an impractical task once thousands of wireless powered sensors are deployed in numerous applications, which makes a battery system not suitable to power wireless self-powered electronic sensors [69]. This raises the demand for devices that are able to power these sensors by harvesting ambient energy. Electrical energy can be harvested from for example ambient mechanical vibrations, wind and aeroelastic vibrations, thermal energy or solar energy [23]. As wind, thermal and solar power are not much present inside most transportation vehicles, this report will deal on harvesting energy from mechanical vibrations present in the transportation sector.

1.2. Goal

The first research into vibration energy harvesting has been performed by Williams and Yates in 1996 [84], and from then on lots of works have been published on this subject, see fig. 1.1. As reading all these papers will be an undoable task, and because the intended field of application is harvesting energy in the transportation sector, the scope of this report will be limited to this sector only.

The underlying research question in this report is:

> *"What is the current status of vibration energy harvesting in the transportation sector, and which type of harvester performs the best in this sector?"*

The steps that will be taken to answer this research question are provided in the next section.

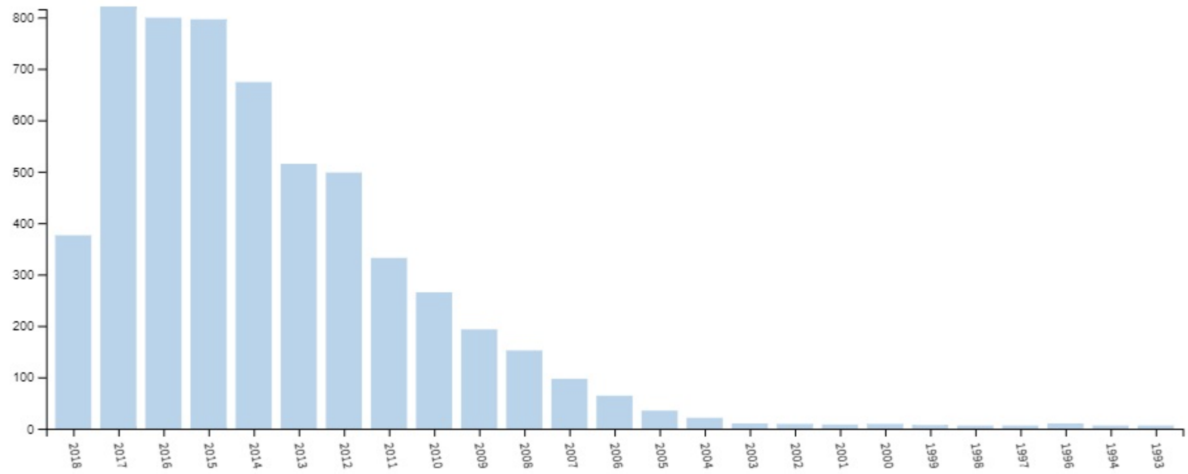

Figure 1.1: Papers published on 'vibration energy harvesting' per year. Graph created on July 9th, 2018 by Web of Science [2].

1.3. Structure of paper

In chapter 2 the operating conditions and requirements for energy harvesters in the transportation sector are discussed (block 1 in fig. A.1 in appendix A). In chapter 3 the four main used transduction mechanisms to convert mechanical energy to electrical energy are discussed, and the preferred electromagnetic transduction mechanism is chosen, after which the basic principles of electromagnetic energy harvesting are discussed in chapter 4 (blocks 2 and 3 in fig. A.1). Literature discussing energy harvesting in the transportation sector is discussed in chapter 5 (blocks 4 and 5 in fig. A.1). This report will finish with a conclusion in chapter 6 where one or more research gaps will be identified. This is block 6 in fig. A.1. At the end of this report a list of used literature is presented, and data or figures that are too big to include in text are provided in several appendices.

2

Problem Definition

As shown in the previous chapter, a lot of works are published on vibration energy harvesting. In a lot of articles new or more efficient techniques are proposed, and prototypes are tested, but most often these works lack reasoning for the design steps taken. Spreemann and Manoli already mentioned this in 2012 [72, p.11]: "Usually the approach is to first build up the transducer and afterwards adjust the vibration to the resonance frequency of the transducer for experimental characterization. In application oriented developments one needs to go the other way round, which definitely brings further challenges in the design process." To prevent producing an energy harvester that is not designed particularly for the specific transportation sector, the requirements for energy harvesters in the transportation sector will be discussed first. Because this report mainly reviews literature and deals about the basic principles of energy harvesting, only requirements that will influence the very conceptual design will be discussed here. In the following sections the vibration characteristics, the mounting and the desired lifespan of energy harvesters in the transportation sector will be discussed.

2.1. Vibration characteristics

In this section the vibration characteristics from railway and automotive transportation applications will be discussed. Vibration characteristics for railway applications are based on a norm describing these vibrations. Vibration characteristics for automotive applications are based on measurements.

2.1.1. Railway vibration characteristics

The international standard *Railway applications - Rolling stock equipment - Shock and vibration tests* [1] specifies the requirements for testing equipment that is to be mounted on railway vehicles and are subjected to shocks and vibrations owing to the nature of railway operational environment. The standard defines three categories in which train vibrations can be divided, and thus three locations where energy harvesters can be mounted. The first category is body mounted, which can be subdivided into two classes: cubicles, subassemblies, equipment and components mounted directly on or under the car body (class A), and anything mounted inside an equipment case which is in turn mounted directly on or under the car body (class B). The second category contains equipment which is mounted to the bogie of the vehicle. The last category involves axle mounted, i.e. mounted to the wheel set assembly of the railway vehicle, sub assemblies, equipment or components. Figure 2.1 provides a visual overview of the three categories. As this report focusses on placing vibration energy harvesters in transportation containers and passenger train cabins, only the vibrations characteristics from the first category will be taken into account. The norm provides information regarding vibrations present in the different categories, so that equipment that is to be mounted on trains can be tested. This means the vibrations described can also be used to design an energy harvester that is to be mounted in one of these categories. An overview of the root mean square (RMS) accelerations present in classes A and B of the used category 1 are presented in table 2.1. As the mass of the energy harvester to be developed will in all probability be less than 500 kg, these accelerations will be present in the region from 5 to 150 Hz [1, fig.2].

Figure 2.1: Three categories in which train vibrations can be divided, and from which energy can be harvested. Category 1: body mounted, category 2: bogie mounted, category 3: axle mounted, [1]. Image taken from [85].

Table 2.1: Functional random vibration test conditions representing vibrations present in body mounted equipment in trains and railway vehicles, [1, Ch.8].

Class	Orientation	RMS acceleration in $\mathrm{m\,s^{-2}}$	RMS acceleration in g
A: Directly mounted	Vertical	0.750	0.0765
	Transverse	0.370	0.0377
	Longitudinal	0.500	0.0510
B: Indirectly mounted	Vertical	1.01	0.103
	Transverse	0.450	0.0459
	Longitudinal	0.700	0.0714

2.1.2. Automotive vibration characteristics

Based on information at Kinergizer, general trends with respect to vibrations in the automotive sector were discovered. Dominant frequencies were found in the 0 to 250 Hz region. The root mean square accelerations at the peaks were approximately 1 $\mathrm{m\,s^{-2}}$. It was found that the recorded signals had multiple dominant frequencies for all recordings from transport sector applications.

2.2. Mounting

When relative motion between objects is present, e.g. in the suspension of a vehicle, it is quite easy to harvest energy form this relative motion. An energy harvester with a stator and a moving or rotating part can be fixed to the objects that are moving relatively to each other. See for example [52] where a rotational vibration energy harvester is proposed to generate electrical energy that would else be lost in a mechanical damper. However, there are a lot of positions in the transportation sector where relative motion between objects is most often not possible, because harvesters can only be mounted to one surface or object. Examples are placing energy harvesters in containers, or on separate crates or goods inside a lorry. In this case use has to be made of inertial forces acting on a proof mass that is suspended or free to move inside the energy harvester. To limit the scope of this research, only situations where no relative motion is present will be considered, so only harvesters using the principle of movement due to inertial forces will be reviewed.

2.3. Lifespan

Another demand for an energy harvester in the transportation sector is its life expectancy. As mentioned in chapter 1, one of the key strengths of energy harvesters is that there is no need for maintenance, as is the case when using batteries. At Kinergizer B.V. there is the rule of thumb that an energy harvester should at least last for ten years. When designing an energy harvester, this minimum life span should be taken into consideration when making design choices.

2.4. Conclusion

Vibrations present in applications in the transportation sector generally have low accelerations, i.e. less than 0.1 g. The frequency bandwidths of these signals vary from 0-30 to 0-250 Hz depending on the vehicle. This means the speed of the vibrations will generally be less than $0.1\ \mathrm{m\,s^{-1}}$, which can be considered as low speed vibrations. To meet the demands from the transportation sector, the harvester to be developed should be an inertial harvester having a lifespan of at least ten years.

3 Energy harvesting transduction mechanisms

There are different ways to convert mechanical energy into electrical energy. The four most used transduction mechanisms are piezoelectric, electrostatic, electromagnetic and magnetostrictive energy harvesting. Examples of these harvesting technologies are shown in fig. 3.1. In this chapter these transduction mechanisms will be discussed briefly in the following subsections, and the electromagnetic transduction method will be chosen at the end.

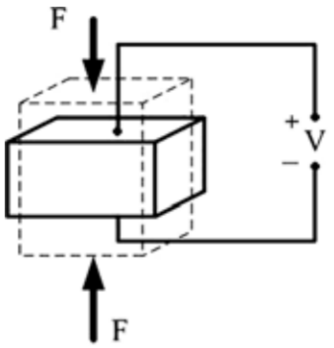

(a) Schematic drawing of piezoelectric energy harvester with F the force exerted on the piezoelectric material, [40].

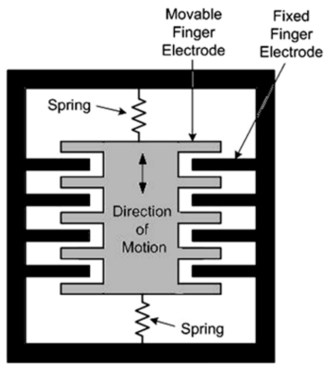

(b) Electrostatic energy harvester concept, [40].

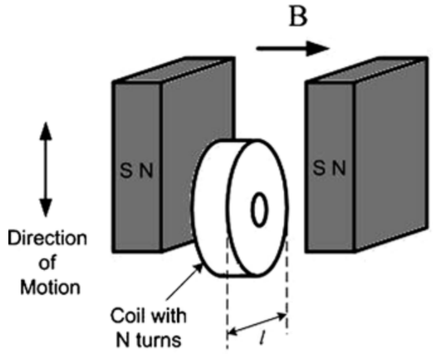

(c) Schematic drawing of an electromagnetic energy harvester. Gray blocks represent permanent magnets, B is the direction of magnetic field lines, [40].

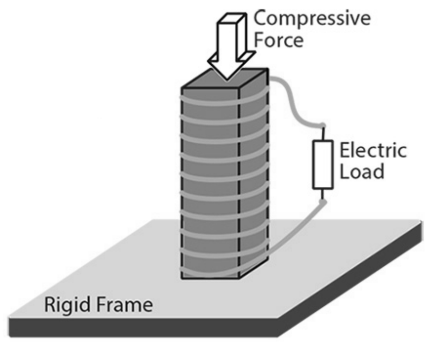

(d) Magnetostrictive harvester principle. The vertical grey beam is made out of magnetostrictive material, around which a coil is wound, [24].

Figure 3.1: Different energy harvesting technologies.

3.1. Piezoelectric energy harvesting

Piezoelectric generators use the ability of some materials that generate charge when stretched mechanically. A schematic drawing of this concept is shown in fig. 3.1a. The damping force in piezoelectric generators is proportional to the speed at which the piezoelectric material is deformed [47]. This type of harvester is mostly used in small scale harvesting applications [9, 48]. An advantage of piezoelectric harvesters is their relatively simple structure [40, 41]. A disadvantage is the fact that mechanical properties may limit the performance and lifespan of piezoelectric harvesters [9, 40]. This is because the brittle material is affected by mechanical fatigue, which causes its failure with the accumulation of loading cycles [26]. These cracks cause a considerable drop in output voltage [7].

3.2. Electrostatic energy harvesting

An electrostatic generator consists of a variable capacitance structure that is driven by mechanical vibrations, see fig. 3.1b. Electrical energy can be harvested by constraining the capacitor charge. When the capacitance decreases, charge will move from the capacitor to a storage device [40]. The damping force in these type of harvesters is constant during operation [47]. Electrostatic devices are mostly used in small scale harvesting such as micro-electromechanical (MEMS) implementations, and are impractical and inefficient for large machines [48]. An advantage of electrostatic harvesters is their high output voltage. The high output impedance of these harvesters however makes them less suitable as a power supply [9, 40]. Other disadvantages are the fact that parasitic capacitances within the structure can sometimes lead to reduced generator efficiency, there is risk of capacitor electrodes shorting [9] and the initial polarizing charge or voltage required [9, 40, 48].

3.3. Electromagnetic energy harvesting

Electromagnetic generators work according to the principle of Faraday's law of induction, which states that a change of magnetic flux through a coil induces a voltage over the ends of the coil, driving a current in the circuit [48]. An example of this is shown in fig. 3.1c. Then damping force in electromagnetic harvesters is proportional to the relative speed between magnet and coil [47]. Due to strong damping forces, rapid flux changes are required, which are hard to achieve in small geometries or at low frequencies [48]. This makes electromagnetic generators better on macro-scale than on micro-scale [10].

3.4. Magnetostrictive energy harvesting

Magnetostrictive materials deform when placed in a magnetic field, and vice versa [9], and can be used in two ways. First of all they can be used independently, where the magnetostrictive material is deformed and energy can be harvested by placing a conducting loop in the changing magnetic field, see fig. 3.1d. Examples of independently used magnetostrictive materials for energy harvesting applications can be found in [79, 82]. It is however more common to combine magnetostrictive materials with piezoelectric harvesters. In this case the magnetostrictive material is deformed when placed in a variable magnetic field, e.g. by placing it next to a moving magnet. Examples can be found in [9, 23, 53].

The high flexibility of this harvesting principle is one of its main benefits, while disadvantages are the non-linear effects and need for bias magnets when used in combination with piezoelectric materials [40, 82]. Magnetostrictive generators are mainly useful for miniaturized devices. When subjected to ambient vibrations, the energy outcome of these devices is limited [53].

3.5. Hybrid energy harvesting

Hybrid energy harvesting methods are also possible, like the coupled harvesters that combine e.g. piezoelectric electromagnetic harvesting technologies as discussed in [76, 80], [11, Ch.2], or the piezoelectric-magnetostrictive combination discussed in previous section.

3.6. Conclusion

In this chapter the four most used energy harvesting transduction mechanisms have been discussed. In this project, the electromechanical transduction mechanism will be used. The first reason for this is the ease to apply this technique in macro scale. The second is the reliability and durability of these harvesters. Avvari et al. [7] showed that the total fatigue cycles of piezoelectric beams were only 88 million, 20 million, and 6 million for the tested subjects exposed to base excitation levels of respectively 0.4g, 0.5g, and 0.6g. The fact that a continuously operating device at 20 Hz already gives more than 600 million cycles a year, underlines the fact that the piezoelectric transduction mechanism is not suitable to be used in long life applications. Finally, the main focus area and field of expertise of Kinergizer B.V. lies on building electromagnetic energy harvesters. This is also one of the reasons the electromagnetic harvesting principle will be chosen, as both the company's interest lies here and more intellectual property and knowledge about designing electromagnetic energy harvesters is internally available.

4

Electromagnetic energy harvesting principles

In the previous chapter the electromechanical transduction method has been selected. In this chapter the basic principles of electromechanical energy harvesting will be discussed, from which it can be concluded that the power that can be generated by an electromagnetic energy harvester is only dependant on the length and cross sectional area of the harvester device. First the basics of electromagnetic induction are formulated, after which electromagnetic energy harvesting is viewed from the mechanical and electrical perspective in sections 4.2 and 4.3 respectively. Section 4.4 briefly discusses the efficiency of electromagnetic energy harvesters, after which this chapter will end with a conclusion.

4.1. Basics on electromagnetic induction

Faraday's law of electromagnetic induction implies that a potential difference is induced between the ends of an electrical conductor when this conductor is moved relative to a magnetic field. When a coil is moved through a magnetic field, this electromotive force ϵ, which is equal to the induced voltage V over the ends of the coil, is defined as the rate of change of the magnetic flux over time:

$$\epsilon = V = -\frac{\mathrm{d}\Phi}{\mathrm{d}t} = -\frac{\mathrm{d}}{\mathrm{d}t} NBA \sin\alpha \tag{4.1}$$

where Φ is the total flux through the coil in Wb, N is the number of coil windings, B is the magnetic field flux density in T, A is the area of the surface bounded by a single turn in m and α is the angle in rad between the coil area and the magnetic flux lines. Assuming a constant number of coil windings, a constant magnetic field flux density and the movement of the coil being orthogonal to the direction of the magnetic flux lines, eq. (4.1) can be simplified to

$$V = -\beta\dot{z} = -NBl\dot{z} \tag{4.2}$$

with l the length of the coil in m orthogonal to the magnetic flux lines, and z the width of the coil in m parallel to the magnetic flux lines. The over-dot is used as a short hand notation for a time derivative. The electromechanical coupling coefficient β is often used to describe the coupling between the magnet and coil [26].

When an electrical load is connected between both ends of the coil, an induced current will start to flow according to Ohm's law:

$$I_{\text{induced}} = \frac{V}{R_{\text{load}}} \tag{4.3}$$

where I_{induced} is the current through the coil in A and R_{load} is the resistance of the load in Ω assuming an ideal coil having no internal resistance. As current starts to flow in the circuit, this means that moving a coil in a magnetic field can be used as an electrical power source. During this process, energy is extracted or dissipated from the mechanical domain, and converted to the electrical domain. In the two following sections this process of electrical power generation will be studied from respectively the mechanical and electrical point of view.

4.2. Mechanical power dissipation

In the previous section it was shown that energy is extracted or dissipated from the mechanical domain, in order to generate power in the electrical domain. In this section the electromagnetic energy harvester is modelled as a mass spring damper system, and formulas for the dissipated power in the mechanical domain are derived.
In this section the energy harvester configuration from fig. 3.1c is considered, where a coil with a certain mass is suspended between two fixed magnets, and the direction of motion is orthogonal to the direction of magnetic field lines. Because energy is extracted from the mechanical domain, the electromagnetic energy harvesting principle can be modelled as a mechanical damper. The total energy harvester can now be modelled as a simple mass spring damper system like the one depicted in fig. 4.1. The coil which is moving in the magnetic field is modelled as a mass m. The spring with spring constant k represents the suspension of the coil, while the damper with damping constant c represents all losses in the system.

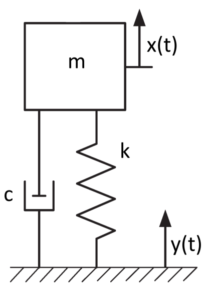

Figure 4.1: Schematic drawing of a mass spring damper system representing the electromagnetic energy harvester from fig. 3.1c where the magnets are fixed to the ground and the coil is able to move relatively to the ground. $y(t)$ is the base excitation, while the position of the coil with mass m is given by $x(t)$. The suspension is modelled by means of a spring and a damper, which are denoted by constants k and c respectively.

For harmonic base excitation with $y(t) = Y\sin(\omega t)$ the governing equation of motion [72, p.14,15] is given as

$$m\ddot{z} + c_{\text{total}}\dot{z} + kz = m\omega^2 Y\sin(\omega t) \tag{4.4}$$

where m is the mass in kg, c_{total} is the total damping constant in $\mathrm{N\,s\,m^{-1}}$, k is the stiffness constant in $\mathrm{N\,m^{-1}}$, ω is the frequency of the input vibration in $\mathrm{rad\,s^{-1}}$ and z is the relative displacement of the mass in m, i.e. $x - y$ where the time dependence of these variables have been left out for readability. The mechanical power that is lost due to damping can be calculated as

$$P_{\text{mech loss}} = F_{\text{damping}}\dot{z} \tag{4.5}$$

where F_{damping} is the force in N exerted on the mass by the damper. This damping force is the product of the damping constant and the relative velocity of the moving mass:

$$F_{\text{damping}} = c_{\text{total}}\dot{z} \tag{4.6}$$

The damping constant c_{total} consists of mechanical damping due to internal friction in the suspension components, aerodynamic damping due to aerodynamic friction between the moving coil and the surrounding air and aerodynamic drag, and electrical damping due to heat losses in the electrical circuit and extraction of generated usable electrical power. This is visualized in fig. 4.2. Note that damping is modelled as a constant here, but in reality the damping will be a function of the speed of the moving mass.

The induced current I from eq. (4.3) creates a electromagnetic force F_{em} opposing the motion of the coil according to Lenz's law. The power that is extracted from the mechanical domain and converted to the electrical domain can be calculated by multiplying only this electromagnetic force F_{em} with the speed of the coil:

$$P_{\text{elec}} = F_{\text{em}}\dot{z} = c_{\text{electrical}}\dot{z}^2 \tag{4.7}$$

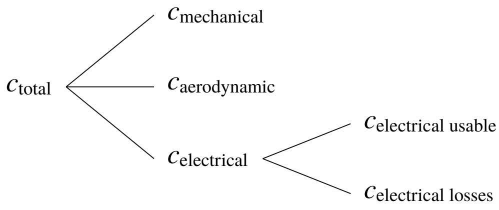

Figure 4.2: Components of the total damping coefficient.

The electromechanical damping constant $c_{\text{electrical}}$ consists of all damping due to moving conducting elements in the magnetic field, i.e. it is the third branch from fig. 4.2, containing both damping due to generation of usable electrical power and damping due to losses in the electrical circuit.

4.3. Electrical power generation

In this section the generated electrical power will be formulated from the electrical domain's perspective. Using Joule's law for electrical power and Ohm's law together with the simplified version of Faraday's law from eq. (4.2) gives the formula for electrical power as [59, p.130-132]:

$$P_{\text{elec}} = I^2 R_{\text{total}} = \frac{V^2}{R_{\text{total}}} = \frac{V^2}{R_{\text{load}} + R_{\text{coil}} + Z_L} = \frac{(NBl\dot{z})^2}{R_{\text{load}} + R_{\text{coil}} + Z_L} \tag{4.8}$$

where Z_L is the coil impedance in Ω, defined as $Z_L = j(2\pi f)L$ with f the frequency of the alternating current in Hz and L the coil inductance in H [43, Ch.3]. At frequencies less than 1 kHz the inductance can be neglected as the resistive impedance of the coil at low frequencies is always significantly larger than the inductive impedance [59, p.134]. Because both the load resistance and the coil resistance and impedance occur in this formula, this means that this general formula for electrical power again consists of both usable electrical power and electrical losses. As eqs. (4.7) and (4.8) both describe the same generated electrical power, the components of the electromechanical damping constant can be extracted by combining these two [26]:

$$c_{\text{electrical}} = \frac{(NBl)^2}{R_{\text{load}} + R_{\text{coil}} + Z_L} \approx \frac{(NBl)^2}{R_{\text{load}} + R_{\text{coil}}} \tag{4.9}$$

which shows that the electromechanical damping constant depends on the coil parameters and the flux linkage.
If one wants to maximize the generated electrical power, it would be too hasty to conclude that both c_{em} and $\dot{z}$ can be maximized for maximum power generation. This is because these parameters are dependant on each other: when damping is increased, the speed of the moving mass will be reduced. This can be visualized by calculating the steady state motion [72, p.14-16] for Equation (4.4):

$$z = Z\sin(\omega t - \phi) \tag{4.10}$$

where

$$Z = \frac{m\omega^2 Y}{\sqrt{\left(k - \omega^2 m\right)^2 + c_{\text{em}}^2\omega^2}} \tag{4.11}$$

When taking the derivative of eq. (4.10) it can easily be shown that the speed is also dependant on the damping present in the system. Many authors have used these steady state motion formulas to derive expressions for maximum power that are not dependant on the relative speed $\dot{z}$ between the base and oscillating mass, like is the case in eqs. (4.7) and (4.8). This is often achieved by combining eq. (4.7) with eqs. (4.10) and (4.11), as the latter two formulas express the relation between these parameters. An example is the following formula derived by Stephen [74]:

$$P_{\text{average}} = \frac{\omega_n^3 m Y}{2\zeta} \tag{4.12}$$

where $\zeta = \frac{c_{em}}{2m\omega_n}$ is the damping ratio and $\omega_n = \sqrt{k/m}$ is the natural frequency of the mass spring damper system. Other examples for similar derived formulas for maximum or average power can be found in [59, p.140-145] [72, p.27] [9, 84], ranging from simple to rather complex formulas for generated electrical power. These formulas lead to the formulation of optimal design parameters for maximum generated power, on which several studies have been performed. Beeby et al. [10] for example stated that maximum electrical power is extracted when electromagnetic damping is equal to mechanical damping. This rule of thumb is also used by e.g. [59, p.145], [40, p.5-7] and [10].
The problem with these formulas is that they are derived for specific cases, and are not validated for the entire range of applications. One assumption that had to be made in order to derive these formulas is that the base excitation is purely harmonic. In most practical situations vibrations are rather random than purely harmonic, as discussed in chapter 2. Having random vibrations as an input for the energy harvester means eq. (4.4) has to be rewritten in a more general form [9]:

$$m\ddot{z} + c_{\text{total}}\dot{z} + kz = -m\ddot{y} \tag{4.13}$$

from which it is harder to analytically derive an expression for the harvested power. Equations (4.7) and (4.8) are still valid, but eq. (4.12) is not valid any more with the absence of a fixed input amplitude and frequency. Another aspect that is often not taken into account when deriving formulas or maximum or average power is the fact that the amplitude of the moving mass will be restrained in most practical situations, as the total dimensions of the harvester will be limited. This means the damping constant cannot be arbitrary small, as this will either mean a huge harvester will be needed, or collisions between the harvester mass and the walls of the harvester will take place, which is inherent to energy loss. Alberda [6] showed that there is a maximum harvestable power for a given device length, and experimentally derives formulas for optimal stroke and damping. In fig. 4.3 the maximum output power per kilogram is plotted against the length of the device. It shows that for a greater device length, more power can be harvested. In [6] it is also stated that, based on

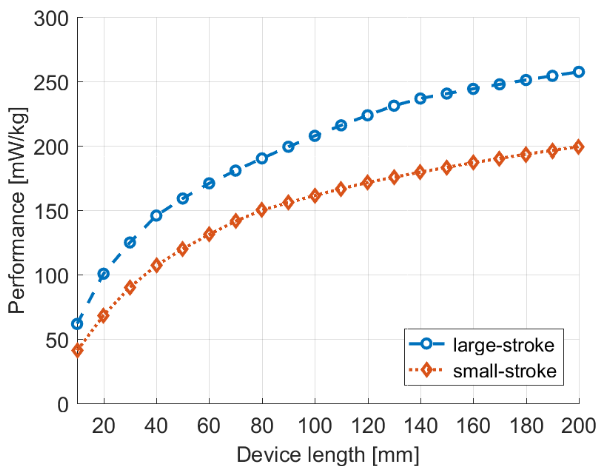

Figure 4.3: Maximum performance of an energy harvester versus device length, [6]. Small stroke devices are designed to achieve 90% of the maximum power that can be generated by large stroke devices.

[15], the harvested power is linear with the proof mass. This can be explained as following: from eq. (4.7) can be concluded that the generated power scales with the damping constant, but only if the relative speed between coil and magnet would not be changed. By increasing the mass of the harvester, more energy can be extracted from the system without influencing the stroke or speed of the harvester mass. This means that the maximum output power will scale linear with the moving mass, which has also been proved by the author by means of numerical modelling.[1] In fig. 4.4 a schematic drawing is provided of an energy harvester showing its dimensions in terms of length and cross sectional area. It can be concluded that the harvestable

[1] Electromagnetic energy harvester simulations have been performed by the author. The principle of these simulations lies in the numerical integration of eq. (4.13). Real life vibration measurements are given as an input ($\ddot{y}$ in eq. (4.13)). Parasitic damping is neglected in this model, i.e. $c_{\text{total}} = c_{\text{electrical}}$, see fig. 4.2. Output power is compared when scaling the harvester's mass while $\frac{m}{c_{\text{electrical}}}$ = constant. The numerical model has been validated by comparing simulated power with experimentally measured power generated by prototypes built by Kinergizer B.V. Errors were in the order of magnitude of a few percent.

energy from an electromagnetic energy harvester only depends on the length and the cross sectional area of the harvester:

- When increasing the length, either mass can be added in this direction, or the stroke can be increased, both of which will increase the output power. The latter only holds to a certain extend: if the stroke of an undamped harvester is not limited by the dimensions of the harvester, further increasing the device length without increasing the fraction of the length occupied by the oscillating mass does not make any sense as this will not further increase the stroke.

- Increasing the cross sectional area of the harvester, i.e. bigger dimensions orthogonal to the direction of the main vibrations allows for a bigger mass, which means larger damping force can be used without influencing the speed of the oscillating mass.

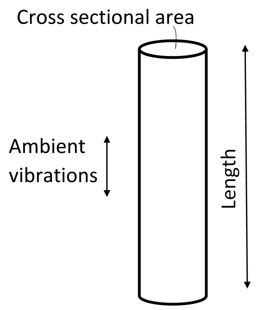

Figure 4.4: Schematic drawing of an energy harvester showing the length and cross sectional area. The harvester's moving mass moves vertically in this drawing, i.e. over the length of the device. Both the length and cross sectional area determine the maximum amount of power that can be scavenged by the harvester.

4.4. Electromagnetic energy harvester efficiency

As the maximum power that can be scavenged by an energy harvester is only dependant on the dimensions of the harvester, designing an energy harvester would be quite straightforward. Harvesting efficiency has however not been taken into account yet. So besides increasing the length or cross sectional area of the harvester in order to increase output power, one could also focus on increasing the harvester's efficiency. First of all effort can be put into reducing the the parasitic losses due to mechanical and aerodynamic losses, see fig. 4.2. Secondly the efficiency can be improved by harvesting at higher output voltages. Both the losses in electrical wire, which scale quadratically with the current through that wire, and the losses in the electrical components, see fig. 4.5, will be decreased.

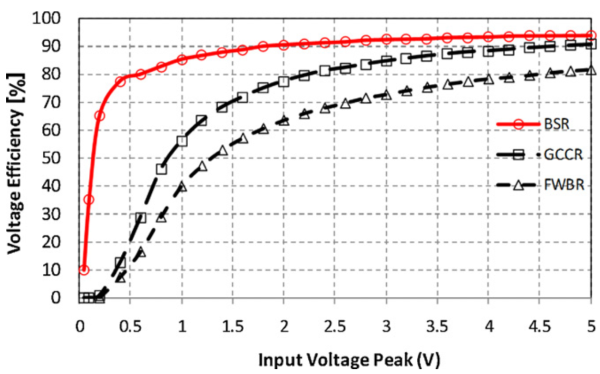

Figure 4.5: Efficiency of three types of rectifying bridges as a function of input voltage peak. Simulated results of the boot strap rectification (BSR) bridge proposed by Rahimi et al. [61] are compared to the most widely used full wave bridge rectifier (FWBR) and a gate cross coupled rectifier (GCCR). Different sinusoidal input voltage peak values are used at a frequency of 1 kHz for the no load output case. Image taken from [61].

4.5. Conclusion

From this chapter it can be concluded that it is hard to derive formulas for the power generated by electromagnetic harvesters from random vibration signals. As a rule of thumb, it can be stated that the output power scales with the stroke of the oscillating mass, and the magnitude of the oscillating mass. As both increasing the mass and increasing the stroke will require more space, it can be concluded that the harvestable power from an electromagnetic energy harvester is bound by its length and cross sectional area. Output power can be increased by either increasing the dimensions of the harvester, or by increasing its efficiency.

5

Literature review

As already said in chapters 1 and 2, this report will mainly focus on works published on vibration energy harvesting in the transportation sector. The scope is was further narrowed by only looking at energy harvesting from the sprung mass, so harvesting from axles, suspensions and bogies etcetera will not be considered here. In this chapter a search for articles published on this topic is performed, and results are analysed in section 5.1. In section 5.2 a look will be taken outside the transportation sector to see if other techniques or approaches exist that have not been applied in the transportation sector. The reviews in sections 5.1 and 5.2 will only be descriptive. In section 5.3 the discussed literature is evaluated, after which this chapter will end with a conclusion.

5.1. Energy harvesting in the transportation sector

The WorldCat, Scopus and Google Scholar search engines have been used to find works published on this topic. The keywords *vibration* and *motion* together with *energy harvesting*, *energy pumping* and *energy scavenging* are used to find the right type of harvesters. To cover as much articles as possible that deal with energy harvesting in the transportation sector, keywords *transport*, *transportation*, *bus*, *train*, *carriage*, *wagon*, *lorry*, *truck*, *trailer* and *container* are used. This gives a set of 28 articles, of which seven are journal articles and twenty-one are conference proceedings. From these articles, eleven discuss energy harvesting in the railway sector, and seventeen write about energy harvesting in the automotive sector. Figure 5.1 gives an overview of the number of publications per year on this subject. Works found are up to ten years old.

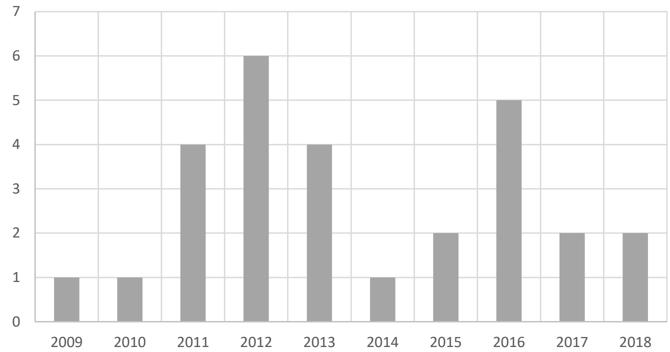

Figure 5.1: Publications per year on vibration energy harvesting from sprung masses in the transportation sector.

In fig. 5.2 the energy harvesters proposed in the found articles are categorised based on different characteristics. A complete overview of all reviewed articles together with their characteristics and relevant parameters can be found in appendix B.

Almost two thirds of the authors designed or applied an piezoelectric energy harvester. No reliability tests

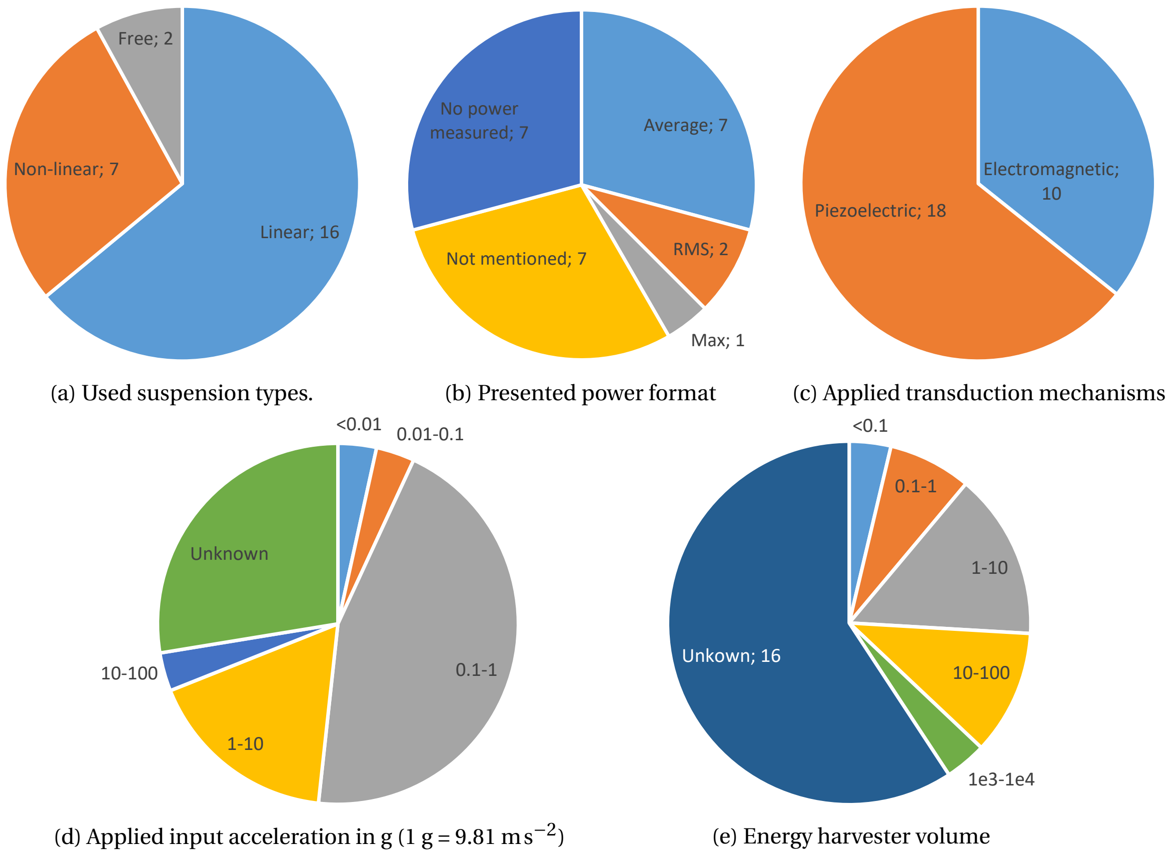

Figure 5.2: Different characteristics of the reviewed vibration energy harvesters in the transportation sector.

have been performed by any of them however, which makes it hard to estimate whether these harvesters will last long enough to meet the requirements discussed in chapter 2. Because no proof regarding the lifespan of piezoelectric harvesters is provided in the reviewed articles, there will be held to the conclusions made in chapter 3, i.e. the choice of transduction mechanism will be on the electromagnetic energy harvesting principle. This will not make reviewing papers discussing piezoelectric harvesting useless, as they can still provide useful information regarding measured vibrations, characteristics like the type of suspension or a measure for output power that can be used as a reference.

Vibration analysis In contrast to most of the articles written on vibration energy harvesting in general (see chapter 2), most articles discussing energy harvesting in the transportation sector do perform a vibration analysis prior to the design of the harvester. The professionality and reliability however differs from author to author. Mouapi et al. for example just uses an iPhone to measure car and train vibrations in [50] and [51] respectively, while other authors like Cho et al. use professional measurement equipment [17].

Design optimization In most articles the proposed designs are not optimized for maximum power output per volume or mass. Some authors do not even design an energy harvester themselves, but use an off the shelf harvester instead, like done in [16, 49, 55, 68]. In some cases the off the shelf harvesters are tuned to dominant frequencies present, but in other cases these off the shelf harvesters are applied without even tuning them. Authors that do develop their own energy harvester most often still do not optimize their design and use a rather basic harvesting concept. Examples are the electromagnetic harvester from [13] where a suspended coil moves relative to a fixed magnet, or the cantilever beam with piezoelectric composite layer from [50]. In [17] the developed piezoelectric harvester has been optimized, however this has not been done in the design phase, but by experimentally modifying different parameters of a prototype.

Suspension type Figure 5.2a shows the suspension types used in the reviewed articles. Three different suspension types are used: linear suspensions, free or zero stiffness suspensions as designed by [21, 86] and non-linear suspensions. Most linear suspensions have one fixed eigenfrequency, which is tuned to the most dominant frequency present in the measured signal. The problem with resonant harvesters is that resonant vibration conversion is inherently limited to narrow band operation [72, p.10], as power is mainly harvested around the resonant frequency, and much less power is harvested at off-resonant frequencies. Several authors have tried to overcome this problem by designing energy harvesters having a non-linear stiffness suspension. The articles using non-linearities in their design are the following:
In [26] and [73] a non-linear hardening behaviour is created by levitating an oscillating magnet on one or between two stationary magnets, like is shown in fig. 5.3.
In [33] a magnetic ball is placed on a magnetic table creating a softening behaviour.
Orfei et al. [55] designed a piezoelectric cantilever with attached seismic mass and two permanent stationary magnets which concept is based on [19]. The stiffness characteristics created by Orfei et al. is not discussed in their paper however, and it remains unclear whether a bistable or hardening behaviour is created. In [17] a piezoelectric cantilever with attached tip mass is used in combination with a pendulum magnet. The idea is that more power is generated by the piezoelectric cantilever when combined with this pendulum magnet.

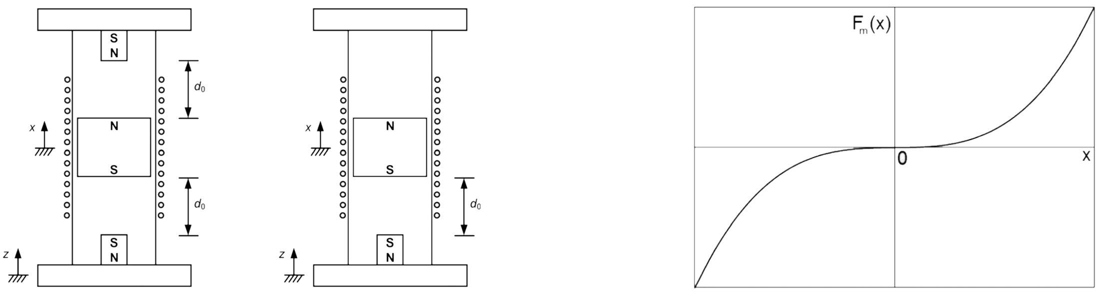

(a) Schematic layout of an energy harvesting with a levitating magnet with double (left) and single levitating configuration inside a cylindrical coil.

(b) Force versus displacement curve showing the hardening behaviour of the magnetic spring design.

Figure 5.3: Non-linear stiffness design with hardening behaviour by De Pasquale et al. [26].

Modality To overcome the previously discussed drawback of having only a small region where energy can be harvested efficiently (i.e. around the harvester's resonant frequency), multimodal harvesters are designed that can harvest efficiently at multiple frequencies. Examples can be found in [28, 34], where structures with multiple dominant eigenfrequencies are used, see fig. 5.4.

(a) Multimodal piezoelectric energy harvester from [28].

(b) Multimodal energy harvester from [34].

Figure 5.4: Multimodal energy harvesting techniques applied in the transportation sector.

Impacts Song et al. [71] describe an energy harvester where steel balls impact on piezoelectric plate. The optimal ball size is determined for this type of harvester, but it is not reasoned why this non-linear method has benefit over using a linear piezoelectric beam.

5.2. Other energy harvesting techniques

Of course the techniques to harvest electrical energy from vibrations as discussed above are not the only options available. That is why some other concepts that claim to improve the energy harvesting efficiency are discussed in this section. If possible, these techniques could also be applied in the transportation sector, although this has not been done yet. As in the previous section, this section will only be descriptive. Techniques that are reviewed are a multistable suspension, the use of impacts, kinematic motion amplification, multimodal harvesting and frequency tuning. This will not be an in-depth review, but rather a brief discussion of existing techniques. Note that this overview will not be complete, as it is undoable to review all works published on energy harvesting, see fig. 1.1. Only the most used energy harvesting techniques or techniques that were promising in the eyes of the author are discussed.

5.2.1. Non-linear stiffness suspension

Apart from the hardening and softening stiffness designs that have been applied in the transportation sector as described in the previous section, a lot of harvesters having bistable or multistable suspensions can be found in literature. An example of a harvester with a bistable magnetic suspension is shown in fig. 5.5a, while mechanical bistable [35] or hybrid suspensions that use a combination of magnetic and mechanical spring elements [54] are also available. A special type of bistable suspension is the harvester consisting of an automatic flipping magnet developed by Paul and George [56]. Multistable suspensions having more then two equilibrium positions are also possible, of which an example is shown in fig. 5.5b.

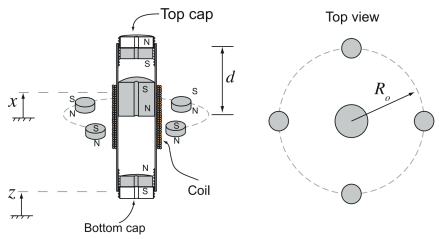

(a) Schematic drawing of a magnetic bistable harvester based on [46].

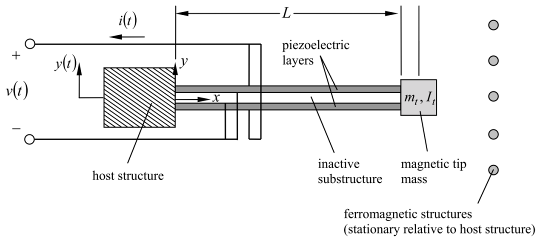

(b) Multistable cantilevered vibration energy harvester, [83].

Figure 5.5: Vibration energy harvester concepts having a bistable or multistable suspension.

5.2.2. Kinematic motion amplification

The idea of kinematic motion amplification is that some kind of lever beam is used to amplify the motion (and thus the velocity) of the harvesting part of the energy harvester. This is explained in fig. 5.6a, where the output motion will be bigger than the input motion. Klein and Zuo have realised a prototype using kinematic motion amplification, see fig. 5.6b. This higher velocity will result in a higher output voltage, which means energy is harvested more efficient (see chapter 4).

5.2.3. Frequency tuning

As discussed in the previous section, energy is harvested in the most efficient way when the eigenfrequency of the energy harvester is equal to the input frequency. One way to be able to harvest maximum energy at multiple frequencies is by changing the eigenfrequency of the energy harvester. Zhu et al. [87] provide an overview of various tuning techniques. Energy harvesters using frequency tuning can be divided into active and passive tuning methods. The actively tuned energy harvesters can be subdivided into two groups: those with continuous tuning and those with intermittent tuning. The former is used for a continuously shifting

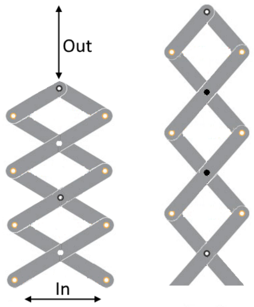

(a) Scissor linkage to amplify motion and velocity, image from [3].

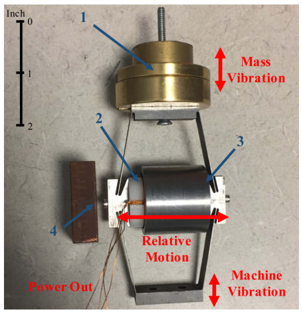

(b) Photograph of harvester with a lever (kinematic) amplification mechanism from [42].

Figure 5.6: The concept of kinematic motion amplification together with a picture of a realized prototype using this principle.

dominant frequency in the vibration signal and has a relatively high energy consumption, while the latter one is applied when there is a slow or seldom shift in excitation frequencies [78]. An example of an active frequency tuning mechanism is shown in fig. 5.7a. A passive frequency tuning mechanism consists of some kind of mechanism that automatically changes the eigenfrequency of the energy harvester when the input frequency changes. An example can be found in fig. 5.7b.

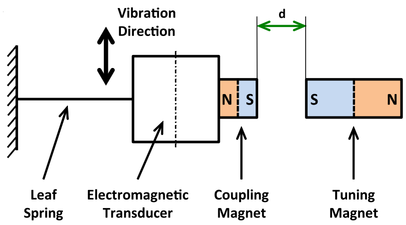

(a) Active tuning mechanism from [37]. The eigenfrequency of the beam can be altered by changing the distance d.

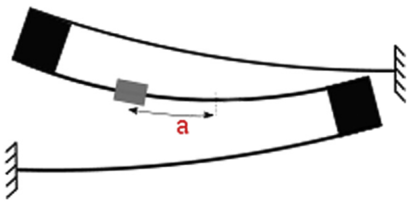

(b) Piezoelectric energy harvester with a passive frequency tuning mechanism [**?**]. The structure's eigenfrequency changes when the mass slides back or forth.

Figure 5.7: Vibration energy harvesters using a frequency tuning mechanism.

5.2.4. Multimodal harvesters

Multimodal harvesters can be divided into single structures having multiple eigenfrequencies relatively close to each other, like shown in fig. 5.4, or multiple oscillating structures with each a different eigenfrequency. Examples of the latter are the array of pendulums from fig. 5.8, the array of multimodal oscillators designed by [67] or the multimodal energy harvester based on magnetic levitation discussed in [4].
In these multimodal designs, structures with different eigenfrequencies are used, so there will be a big range of frequencies in which one of these harvesters will operate in resonance mode. This means more energy can be harvested to harvesters operating off-resonant.

5.2.5. Impacts

Several authors have used the principle of impacting masses when designing an energy harvester. The idea of most impact based vibration energy harvesting devices is that a big mass with low eigenfrequency will impact a smaller mass with high eigenfrequency, see figs. 5.9a and 5.9d. This can be done via direct impact, or indirect impact as the repulsively driven frequency increased generator from Tang et al. [77]. In fig. 5.9e a catch-release or 'plucking' mechanism is used to increase the frequency of the generator cantilever. Plucking excitation implies a slow deflection of the transducer element followed by its sudden release, in contrast to the instantaneous momentum transfer occurring in impact devices [30]. In fig. 5.9b the motion of the smaller

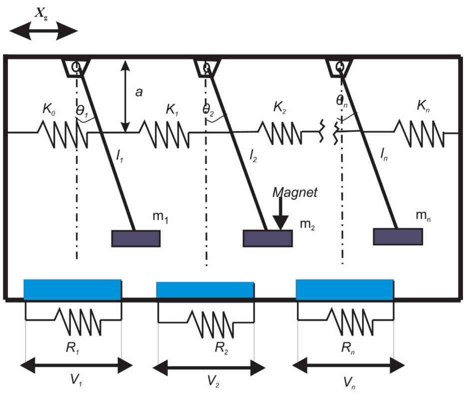

Figure 5.8: Schematic drawing of an array of n pendulum harvesters from [45]. Spring constants k_i can be equal to zero for uncoupled or ungrounded pendulum array harvesters.

mass is rather amplified, while maintaining more or less the same frequency as the big mass. The idea of all these type of harvesters is the same: energy can be harvested more efficient at higher speeds as proven in chapter 2, which would make impact harvesters more efficient than non-impact harvesters.
Besides using impacts to directly increase the frequency of the harvesting mass, they can also be used as part of a winding mechanism. Energy will be stored in a spring during the operation of this type of harvester. When releasing this spring, energy can be harvested from the harvester mass in this device, see fig. 5.9c. Other examples can be found in [36, 75, 81].

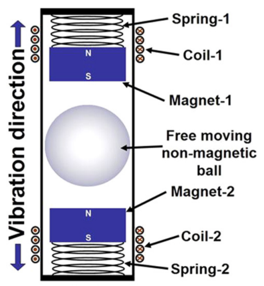

(a) Frequency up-conversion mechanism by means of using an end stop. Schematic drawing from [29].

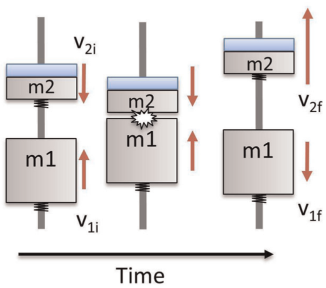

(b) Velocity amplification process through pairwise collision from [20].

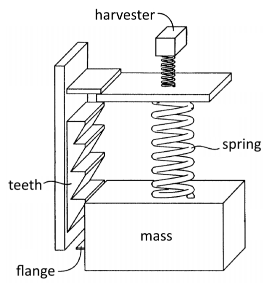

(c) Schematic drawing of a harvester using a winding mechanism. Energy will be harvested from the high frequency vibrations of the little top mass. Image from [38].

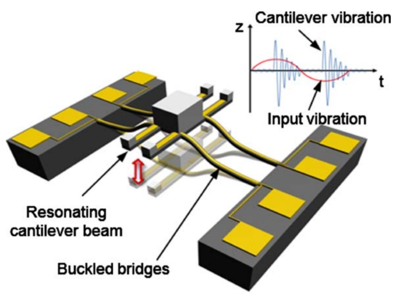

(d) Schematic view of energy harvester using buckled beam impacts [39].

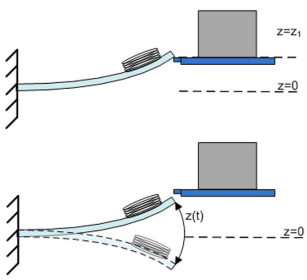

(e) Schematic drawing of a mechanical catch-release or 'plucking' frequency up-conversion mechanism, [89].

Figure 5.9: Different types of harvesters using impacts.

5.3. Performance evaluation

It is remarkable that authors who introduce an energy harvester do not compare their device with other harvesters in terms of power output. The lack of such comparison makes it hard to judge if the proposed design indeed performs better. Several authors underlined the need for a metric or standard to compare energy harvesters [5, 31, 72]. Some authors have proposed metrics to rate energy harvesters, from which the most widespread are the Volume Figure of Merit and Bandwidth Figure of Merit by Mitcheson et al. [48]. Other proposed metrics are for example the dimensionless term for 'effectiveness' by Roundy [65] or the dimensionless performance index by Pellegrini et al. [57].
But the problem is that the data needed in order to calculate these metrics are either not available in a large part of the reviewed articles, or are presented in different formats, see figs. 5.2b, 5.2d and 5.2e. This is not only the case for the articles published on harvesting in the transportation sector, but also for the other reviewed papers. As comparing different concepts by means of a metric is not possible, it is tried to determine the benefits of a certain harvester concepts by logical reasoning. In the following subsections, the previously discussed harvesting concepts are compared to a baseline harvester, consisting of a single mass suspended by a linear monostable suspension.

5.3.1. Non-linear suspension

Based on literature it is hard to determine whether having a non-linear suspension is beneficial compared to a linear suspension or not. In [22] different types of suspension non-linearities are reviewed by Daqaq et al., among which are suspensions with a hardening or softening behaviour and bistable suspensions. In general it is concluded that a hardening stiffness does not have any benefit compared to a linear suspension when it comes to output power, while a softening stiffness or bistable suspension could be beneficial instead. It is however hard to predict how non-linear stiffness suspensions would behave in real life situations, mainly because of the non-uniqueness of solutions. The writers state that it is difficult to have a general prediction regarding the output power of a harvester with a non-linear suspension, and it is easier to determine the efficiency of non-linear harvesters by evaluating their performance on random or real-life signals.
So general research into non-linear suspensions do not provide enough insight into the benefits of using a suspension with non-linear stiffness, but predictions are that non-linearities might be beneficial. This means that the the effect of a non-linear suspension should be studied for this specific case, i.e. energy harvesting in the transportation sector. One possible way of doing this is by performing simulations for specific input vibration signals and comparing different suspension types which can lead to the optimal suspension design for that application.

5.3.2. Kinematic motion amplification

Some articles make it look like more energy can be harvested when using a kinetic amplification mechanism, as this will increase the velocity and thus the generated power of the harvester, see eq. (4.7). This is not true however, because the force applied by the damper will be amplified by the lever beam. This means that, in order to experience the same damping force, the size of the damper has to be divided by the same number as with which the motion is amplified, so no increase of output power will be achieved. Kinematic motion amplification can still be beneficial nonetheless. As discussed in chapter 4, power is harvested more efficient at higher voltages, and the induced voltage scales linear with the relative speed between magnet and coil. With an amplification mechanism, energy could thus be harvested more efficiently, as this mechanism increases the relative speed.
The gain achieved by kinematic motion amplification is limited however, as it only decreases the electrical losses in an energy harvester. As these electrical losses are estimated to be around 10%, the benefit of this harvester cannot be more than that. As the amplification mechanism will also claim some of the design space that could else be used to have a bigger mass or larger stroke, the expectations are that kinematic motion amplification will hardly be beneficial. The only situation where kinematic motion amplification might be advantageous, is when a huge damping force is needed while it will be too costly to create such a big damping force by increasing magnet and coil parameters only. In this case, applying a kinetic motion amplification mechanism will allow for a medium and affordable damper, while applying a high damping force on the moving mass.

5.3.3. Frequency tuning

As said in section 5.2.3, active tuning mechanisms often consume a relatively large amount of power, which makes applying them most likely not profitable. In [66] Roundy and Zhang state that applying an active tuning actuator will never result in a net increase in power output. Because the tuning mechanism will occupy part of the design space, while it also consumes some of the harvested power, the expectation is that active frequency tuning will not be profitable for energy harvesters in the transportation sector.
If one manages to design a proper passive tuning mechanism, this will mean a huge increase in output power, while consuming zero power for actuation. The problem is that it is hard to design a proper passive tuning mechanism that will not use the entire design space. Another issue is that the energy harvester must be robust, as it should last for at least 10 years (chapter 2). Sliding or impacting masses will reduce the lifetime of the harvester, making passive frequency tuning less desirable for this application field.

5.3.4. Multimodal harvesters

A multimodal harvester can be beneficial when the vibration signal consists of two or more dominant frequencies, see chapter 2. This way energy from all these frequency peaks could efficiently be harvested. The drawback is that both the multimodal design itself and the sophisticated interface circuit required will occupy a big part of the design space. This means that for each specific case the consideration has to be made whether the output power is maximized when having a big single modal harvester able to harvest efficient at one frequency or by having a multimodal harvester consisting of two or more smaller masses that harvest less energy than the big one, but is efficient at multiple frequencies. For each specific application this analysis should be performed.

5.3.5. Impacts

The use of impacts will be inherently associated with energy losses, as coefficients of restitution of 1 do not exist in practice. In some cases it might be beneficial to use impacts in a vibration energy harvester design, but the field where this principle is beneficial is that of applications having a maximum stroke which is way lower than the amplitude of the ambient input vibrations [32] [12, p.46-61]. This will not be the case in the transportation sector, as the designated design space for an energy harvester is expected to be big enough to design a harvester having a stroke of the same magnitude as the amplitude of the input vibration signal. The use of impacts will thus not make any sense when designing a harvester for the transportation sector.

5.4. Conclusion

As a conclusion, for energy harvesting in transportation sector it can be said that most authors do a vibration analysis and tune the eigenfrequency of their harvester to one of the dominant frequencies present in the signal. Energy harvesters in the transportation sector are often not optimized however, while optimizing for example the coupling architecture (magnet, coil and back iron components if existent) [72], or mass and stroke [6] will increase the power output.
Several techniques that claimed to improve the output power were discussed. It turned out that harvesters using a kinematic motion amplification system, a frequency tuning system or harvesters that made use of impacts do not have higher output power when applied in the transportation sector. Multimodal harvesting techniques seem promising when electrical energy is to be harvested from vibrations having multiple dominant frequencies. Designing an energy harvester having a non-linear suspension could have benefits when it comes to output power, although it is unclear how much the output will increase.

6

Conclusion

In this chapter the final conclusions will be presented to summarize the performed literature review.
The four most used energy harvesting transduction mechanisms, i.e. the piezoelectric, electrostatic, electromagnetic and magnetostrictive mechanism have been studied. For vibration energy harvesting in the transportation sector, electromagnetic energy harvesting is the preferred transduction method.
The output power of an electromagnetic energy harvester is determined by the stroke and mass of the harvester and its efficiency. This means that the length and cross sectional area determine the harvester's output power, together with the mechanical and electrical losses. As vibrations in transportation sector application predominantly exist of low frequencies and low accelerations, the induced voltage by an electromagnetic transducer will be relatively low due to the low speed between coil and magnet.
A literature study has shown that most harvesters developed for the transportation sector are not optimized for maximum performance. It is expected that a lot of profit can be gained when optimizing an energy harvester for one or more specific applications. Also the benefits of using different harvesting techniques such as a multimodal harvester or having a non-linear suspension are barely discussed. As vibrations present in transportation applications consist of multiple dominant frequencies (see chapter 2), the interest of the author especially goes to harvesting energy from multiple frequencies. This brings up the following research question:

> *"In terms of output power, what are the benefits of a multiple degree of freedom electromagnetic vibration energy harvester with respect to a single degree of freedom harvester for applications in the transportation sector?"*

The steps that need to be taken in order to answer this research question are steps 7 till 15 from the work flow diagram in fig. A.1 in appendix A. These steps will be worked out in a thesis report by the same author.

Bibliography

[1] Railway applications - rolling stock equipment - shock and vibration tests, 2010.

[2] Web of science, 2018. URL `https://www.webofknowledge.com`. Accessed: 09-07-2018.

[3] Scissor lifts information, 2018. URL `https://www.globalspec.com/learnmore/material_handling_packaging_equipment/material_handling_equipment/scissor_lifts`. Accessed: 09-06-2018.

[4] I. Abed, N. Kacem, N. Bouhaddi, and M. L. Bouazizi. Multi-modal vibration energy harvesting approach based on nonlinear oscillator arrays under magnetic levitation. *Smart Materials and Structures*, 25(2): 025018, 2016.

[5] A. R. Akande, Action Nechibvute, and P. V. C. Luhanga. Characterization of piezoelectric energy harvesting devices: Need for a standard. In *Power and Energy Systems*, 2010.

[6] R. Alberda. Parameter study of velocity-damped vibration energy harvesters in low frequency and wide bandwidth operation. Thesis, Delft University of Technology, 2016.

[7] Panduranga Vittal Avvari, Yaowen Yang, and Chee Kiong Soh. Long-term fatigue behavior of a cantilever piezoelectric energy harvester. *Journal of Intelligent Material Systems and Structures*, 28(9):1188–1210, 2017.

[8] M. Baldauf, P. Fidler, T. Keutel, and O. Kanoun. Method for application specific electrodynamic harvester design. In *Eighth International Multi-Conference on Systems, Signals & Devices*, pages 1–2, 2011.

[9] S. P. Beeby, M. J. Tudor, and N. M. White. Energy harvesting vibration sources for microsystems applications. *Measurement Science and Technology*, 17(12):R175, 2006.

[10] S. P. Beeby, M. J. Tudor, R. N. Torah, S. Roberts, T. O'Donnell, and S. Roy. Experimental comparison of macro and micro scale electromagnetic vibration powered generators. *Microsystem Technologies*, 13(11): 1647–1653, 2007.

[11] Nicu Bizon, Naser Mahdavi Tabatabaei, Frede Blaabjerg, and Erol Kurt. *Energy Harvesting and Energy Efficiency*. Springer, 2017.

[12] T.W.A. Blad. Vibration energy harvesting from human motion. Thesis, Delft University of Technology, 2017.

[13] S. Bradai, S. Naifar, C. Viehweger, and O. Kanoun. Electromagnetic vibration energy harvesting for railway applications. volume 148, 2018.

[14] O. Brignole, C. Cavalletti, A. Maresca, N. Mazzino, M. Balato, A. Buonomo, L. Costanzo, M. Giorgio, R. Langella, A. L. Schiavo, A. Testa, and M. Vitelli. Resonant electromagnetic vibration harvesters feeding sensor nodes for real-time diagnostics and monitoring in railway vehicles for goods transportation: A numerical-experimental analysis. pages 456–461, 2016.

[15] T. von Buren, P. D. Mitcheson, T. C. Green, E. M. Yeatman, A. S. Holmes, and G. Troster. Optimization of inertial micropower generators for human walking motion. *IEEE Sensors Journal*, 6(1):28–38, 2006.

[16] M. H. Chan. Low-grade waste vibration energy recovery from hong kong franchised buses. *International Journal of Green Energy*, 11(4):431–437, 2014.

[17] J. Y. Cho, S. Jeong, H. Jabbar, Y. Song, J. H. Ahn, J. H. Kim, H. J. Jung, H. H. Yoo, and T. H. Sung. Piezoelectric energy harvesting system with magnetic pendulum movement for self-powered safety sensor of trains. *Sensors and Actuators, A: Physical*, 250:210–218, 2016.

[18] U. C. Chukwu and S. M. Mahajan. Piezoelectric energy-scavenging possibilities in vehicular systems for powering ulpt. In *2017 IEEE Power & Energy Society General Meeting*, pages 1–8, 2017.

[19] F. Cottone, H. Vocca, and L. Gammaitoni. Nonlinear energy harvesting. *Physical Review Letters*, 102(8): 080601, 2009.

[20] Francesco Cottone, Ronan Frizzell, Suresh Goyal, Gerard Kelly, and Jeff Punch. Enhanced vibrational energy harvester based on velocity amplification. *Journal of Intelligent Material Systems and Structures*, 25(4):443–451, 2014.

[21] M Cueff and S Basrour. A multi degree of freedom vibration magnetic energy harvester for transport application. In *Journal of Physics: Conference Series*, volume 476, page 012092. IOP Publishing, 2017.

[22] Mohammed F. Daqaq, Ravindra Masana, Alper Erturk, and D. Dane Quinn. On the role of nonlinearities in vibratory energy harvesting: A critical review and discussion. *Applied Mechanics Reviews*, 66(4): 040801–040801–23, 2014.

[23] Joseph Davidson and Changki Mo. Recent advances in energy harvesting technologies for structural health monitoring applications. *Smart Materials Research*, 2014:14, 2014.

[24] Daniele Davino. Kinetic energy harvesting by magnetostrictive materials, 2018. URL `https://www.sigmaaldrich.com/technical-documents/articles/materials-science/kinetic-energy-harvesting.html`. Accessed: 03-05-2018.

[25] G De Pasquale, A Somà, and F Fraccarollo. Piezoelectric energy harvesting for autonomous sensors network on safety-improved railway vehicles. *Proceedings of the Institution of Mechanical Engineers, Part C: Journal of Mechanical Engineering Science*, 226(4):1107–1117, 2012.

[26] G. De Pasquale, A. Somà, and N. Zampieri. Design, simulation, and testing of energy harvesters with magnetic suspensions for the generation of electricity from freight train vibrations. *Journal of Computational and Nonlinear Dynamics*, 7(4), 2012.

[27] Daniele Dondi, Giacomantonio Napoletano, Alessandro Bertacchini, Luca Larcher, and Paolo Pavan. A wsn system powered by vibrations to improve safety of machinery with trailer. In *Sensors, 2012 IEEE*, pages 1–4. IEEE, 2012.

[28] Claudio Gatti, José Ramirez, Mariano Febbo, and Sebastián Machado. Multimodal piezoelectric device for energy harvesting from engine vibration. *Journal of Mechanics of Materials and Structures*, 13(1): 17–34, 2018.

[29] Miah A. Halim and Jae Y. Park. A non-resonant, frequency up-converted electromagnetic energy harvester from human-body-induced vibration for hand-held smart system applications. *Journal of Applied Physics*, 115(9):094901, 2014.

[30] Miah A. Halim, Hyunok Cho, Md Salauddin, and Jae Y. Park. A miniaturized electromagnetic vibration energy harvester using flux-guided magnet stacks for human-body-induced motion. *Sensors and Actuators A: Physical*, 249:23–31, 2016.

[31] R. L. Harne and K. W. Wang. A review of the recent research on vibration energy harvesting via bistable systems. *Smart Materials and Structures*, 22(2):023001, 2013.

[32] Ahmed Haroun, Ichiro Yamada, and Shinichi Warisawa. Micro electromagnetic vibration energy harvester based on combined free/impact motion for low frequency-large amplitude operation. In *ASME 2017 International Mechanical Engineering Congress and Exposition*, volume 10, page V010T13A023, Volume 10: Micro- and Nano-Systems Engineering and Packaging, 2017. ASME.

[33] G. A. Hart, S. D. Moss, D. J. Nagle, G. Jung, A. R. Wilson, C. Ung, W. K. Chiu, and G. Crew. Vibration energy harvesting for aircraft, trains and boats. pages 136–142, 2013.

[34] S. Hashimoto, N. Nagai, Y. Fujikura, J. Takahashi, S. Kumagai, M. Kasai, K. Suto, and H. Okada. Development of a power generation device for multi-mode vibration in automobiles. In *The 2012 International Conference on Advanced Mechatronic Systems*, pages 134–138, 2012.

[35] Justus Laurens Herder and Nima Tolou. Energy harvester. United States Patent US20150180374A1, 2015.

[36] Frances A. Hill, Timothy F. Havel, David Lashmore, Mark Schauer, and Carol Livermore. Storing energy and powering small systems with mechanical springs made of carbon nanotube yarn. *Energy*, 76:318–325, 2014.

[37] D. Hoffmann, A. Willmann, T. Hehn, B. Folkmer, and Y. Manoli. A self-adaptive energy harvesting system. *Smart Materials and Structures*, 25(3):035013, 2016.

[38] Ronald Scott Jackson, John F. Gardner, and David Harris. System for generating electrical energy form ambient energy. United States Patent US 8,030,786 B2, 2008.

[39] Seok-Min Jung and Kwang-Seok Yun. Energy-harvesting device with mechanical frequency-up conversion mechanism for increased power efficiency and wideband operation. *Applied Physics Letters*, 96(11): 111906, 2010.

[40] T.J. Kazmierski and S. Beeby. *Energy Harvesting Systems; Principles, Modeling and Applications*. Springer, 2011.

[41] A. Khaligh, P. Zeng, and C. Zheng. Kinetic energy harvesting using piezoelectric and electromagnetic technologies; state of the art. *IEEE TRANSACTIONS ON INDUSTRIAL ELECTRONICS*, 57(3):850–860, 2010.

[42] J. Klein and L. Zuo. A velocity-amplified electromagnetic energy harvester for small amplitude vibration. *Smart Materials and Structures*, 26(9):095057, 2017.

[43] Tony R. Kuphaldt. *Lessons in electric circuits*, volume 2. Koros Press, 2002.

[44] Florian Maier, Michael Sturmlechner, and Stefan Dierneder. Novel energy harvester with low friction losses. In *Systems, Signals and Devices, 2009. SSD'09. 6th International Multi-Conference on*, pages 1–6. IEEE, 2009.

[45] P. V. Malaji and Shaikh Faruque Ali. Broadband energy harvesting with mechanically coupled harvesters. *Sensors and Actuators A: Physical*, 255:1–9, 2017.

[46] B. P. Mann and B. A. Owens. Investigations of a nonlinear energy harvester with a bistable potential well. *Journal of Sound and Vibration*, 329(9):1215–1226, 2010.

[47] P. D. Mitcheson, T. C. Green, E. M. Yeatman, and A. S. Holmes. Architectures for vibration-driven micropower generators. *Journal of Microelectromechanical Systems*, 13(3):429–440, 2004.

[48] P. D. Mitcheson, E. M. Yeatman, G. K. Rao, A. S. Holmes, and T. C. Green. Energy harvesting from human and machine motion for wireless electronic devices. *Proceedings of the IEEE*, 96(9):1457–1486, 2008.

[49] S. H. Mohamad, A. Z. Jidin, M. F. Yaakub, S. Ahmad, and N. A. N. Azlan. Microgeneration of electrical energy using piezoelectric from car movement. In *2016 IEEE International Conference on Power and Energy (PECon)*, pages 818–822, 2016.

[50] A. Mouapi, N. Hakem, G. Y. Delisle, and N. Kandil. A novel piezoelectric micro-generator to power wireless sensors networks in vehicles. In *2015 IEEE 15th International Conference on Environment and Electrical Engineering (EEEIC)*, pages 1089–1092, 2015.

[51] A. Mouapi, N. Hakem, N. Kandil, and G. V. Kamani. Energy harvesting design for autonomous wireless sensors network applied to trains. volume 2016-November, 2016.

[52] C. Nagode, M. Ahmadian, and S. Taheri. Motion-based energy harvesting devices for railroad applications. (49071):267–271, 2010.

[53] Slim Naifar, Sonia Bradai, Christian Viehweger, and Olfa Kanoun. Survey of electromagnetic and magnetoelectric vibration energy harvesters for low frequency excitation. *Measurement*, 106:251–263, 2017.

[54] Abdullah Nammari and Hamzeh Bardaweel. Design enhancement and non-dimensional analysis of magnetically-levitated nonlinear vibration energy harvesters. *Journal of Intelligent Material Systems and Structures*, 28(19):2810–2822, 2017.

[55] F. Orfei, I. Neri, H. Vocca, and L. Gammaitoni. Nonlinear vibration energy harvesting at work: An application for the automotive sector. In *2013 IEEE International Symposium on Circuits and Systems (ISCAS2013)*, pages 2735–2738, 2013.

[56] R. Paul and B. George. Automatic flipping magnet type electromagnetic energy harvester. *Electronics Letters*, 52(17):1476–1478, 2016.

[57] Sergio P Pellegrini, Nima Tolou, Mark Schenk, and Just L Herder. Bistable vibration energy harvesters: A review. *Journal of Intelligent Material Systems and Structures*, 24(11):1303–1312, 2013.

[58] A. Phipps, D. Phung, M. Kerber, B. Dick, A. Powers, and R. Waters. Development of kinetic energy harvesting systems for vehicle applications. In *2011 IEEE SENSORS Proceedings*, pages 24–27, 2011.

[59] Shashank Priya and Daniel J Inman. *Energy harvesting technologies.* Springer, 2009.

[60] D. Radha, R. Syed Zahid Ali, and T. Yuvaraja. Generation of electricity from vibration of vehicles. In *2017 International Conference on Electrical, Electronics, Communication, Computer, and Optimization Techniques (ICEECCOT)*, pages 405–407, 2017.

[61] Arian Rahimi, Özge Zorlu, Ali Muhtaroğlu, and Haluk Külah. An electromagnetic energy harvesting system for low frequency applications with a passive interface asic in standard cmos. *Sensors and Actuators A: Physical*, 188:158–166, 2012.

[62] M. F. Bin Ab Rahman and S. L. Kok. Investigation of useful ambient vibration sources for the application of energy harvesting. In *2011 IEEE Student Conference on Research and Development*, pages 391–396, 2011.

[63] L. Reynolds and A. Wasenczuk. Energy harvesting for asset condition monitoring and remote sensing in the rail industry. volume 2006, pages 194–197, 2006.

[64] A Romani, C Tamburini, A Golfarelli, R Codeluppi, M Dini, E Sangiorgi, M Tartagni, and RP Paganelli. *Actively controlled power conversion techniques for piezoelectric energy harvesting applications*, volume 54, pages 359–363. Springer, Dordrecht, 2010.

[65] Shad Roundy. On the effectiveness of vibration-based energy harvesting. *Journal of Intelligent Material Systems and Structures*, 16(10):809–823, 2005.

[66] Shad Roundy and Yang Zhang. Toward self-tuning adaptive vibration-based microgenerators. In *Smart Materials, Nano-, and Micro-Smart Systems*, volume 5649, page 12. SPIE, 2005.

[67] I. Sari, T. Balkan, and H. Külah. An electromagnetic micro power generator for low-frequency environmental vibrations based on the frequency upconversion technique. *Journal of Microelectromechanical Systems*, 19(1):14–27, 2010.

[68] S. Scorcioni, A. Bertacchini, D. Dondi, L. Larcher, P. Pavan, and G. Mainardi. A vibration-powered wireless system to enhance safety in agricultural machinery. In *IECON 2011 - 37th Annual Conference of the IEEE Industrial Electronics Society*, pages 3510–3515, 2011.

[69] Abu Raihan Mohammad Siddique, Shohel Mahmud, and Bill van Heyst. A comprehensive review on vibration based micro power generators using electromagnetic and piezoelectric transducer mechanisms. *Energy Conversion and Management*, 106:728–747, 2015.

[70] D. Song, C. H. Yang, S. K. Hong, S. B. Kim, M. S. Woo, and T. H. Sung. Feasibility study on application of piezoelectricity to convert vibrations of korea train express. In *Proceedings of ISAF-ECAPD-PFM 2012*, pages 1–4, 2012.

[71] D. Song, H. Jang, S. B. Kim, and T. H. Sung. Piezoelectric energy harvesting system for the vertical vibration of superconducting maglev train. *Journal of Electroceramics*, 31(1-2):35–41, 2013.

[72] D. Spreemann and Y. Manoli. *Electromagnetic Vibration Energy Harvesting Devices.* Springer, 2012.

[73] J St-John, Panagiotis Alevras, Stephanos Theodossiades, Homer Rahnejat, and P Kelly. Nonlinear energy harvesting from base excitation in automotive applications. 2016.

[74] N. G. Stephen. On energy harvesting from ambient vibration. *Journal of Sound and Vibration*, 293(1): 409–425, 2006.

[75] Khalis Suhaimi, Roszaidi Ramlan, and Azma Putra. Translation to rotary frequency-up conversion vibration based energy harvesting device for human body motion. *Applied Mechanics and Materials*, 471: 349–354, 2014.

[76] Yonas Tadesse, Zhang Shujun, and Shashank Priya. Multimodal energy harvesting system: Piezoelectric and electromagnetic. *Journal of Intelligent Material Systems and Structures*, 20(5):625–632, 2009.

[77] Q. Tang, Y. Yang, and X. Li. Repulsively driven frequency-increased-generators for durable energy harvesting from ultra-low frequency vibration. *The Review of scientific instruments*, 85(4):045004, 2014.

[78] Jens Twiefel and Henrik Westermann. Survey on broadband techniques for vibration energy harvesting. *Journal of Intelligent Material Systems and Structures*, 24(11):1291–1302, 2013.

[79] T. Ueno and S. Yamada. Performance of energy harvester using iron-gallium alloy in free vibration. *IEEE Transactions on Magnetics*, 47(10):2407–2409, 2011.

[80] R. Challa Vinod, M. G. Prasad, and T. Fisher Frank. A coupled piezoelectric-electromagnetic energy harvesting technique for achieving increased power output through damping matching. *Smart Materials and Structures*, 18(9), 2009.

[81] Frans Vromans and Bernardus Johannes Meijer. Equipment is for production of electrical energy from mechanical movement and uses generator with two or more-poled rotor wheel and stator. Dutch Patent NL1032844C2, 2008.

[82] Lei Wang and F. G. Yuan. Vibration energy harvesting by magnetostrictive material. *Smart Materials and Structures*, 17(4), 2008.

[83] A. M. Wickenheiser and E. Garcia. Broadband vibration-based energy harvesting improvement through frequency up-conversion by magnetic excitation. *Smart Materials and Structures*, 19(6):065020, 2010.

[84] C. B. Williams and R. B. Yates. Analysis of a micro-electric generator for microsystems. *SENSORS AND ACTUATORS A*, 52(1/3):8–11, 1996.

[85] Marcus Wong. Bogie beneath a vhqf quarry hopper, 2011. URL `https://railgallery.wongm.com/wagons/vhqf/E110_2970.jpg.html`. Accessed: 05-07-2018.

[86] J. Yeo, H. Park, J. Jo, and Y. Yang. Multi-dimensional vibration energy harvester for efficient use in common environment. In *2015 IEEE SENSORS*, pages 1–4, 2015.

[87] Dibin Zhu, Michael J. Tudor, and Stephen P. Beeby. Strategies for increasing the operating frequency range of vibration energy harvesters: a review. *Measurement Science and Technology*, 21(2):022001, 2010.

[88] Q. Zhu, M. Guan, and Y. He. Vibration energy harvesting in automobiles to power wireless sensors. In *2012 IEEE International Conference on Information and Automation*, pages 349–354, 2012.

[89] Ö. Zorlu, E. T. Topal, and H. Kulah. A vibration-based electromagnetic energy harvester using mechanical frequency up-conversion method. *IEEE Sensors Journal*, 11(2):481–488, 2011.

A

Workflow Diagram

The workflow diagram followed during this research project is depicted in Figure A.1.

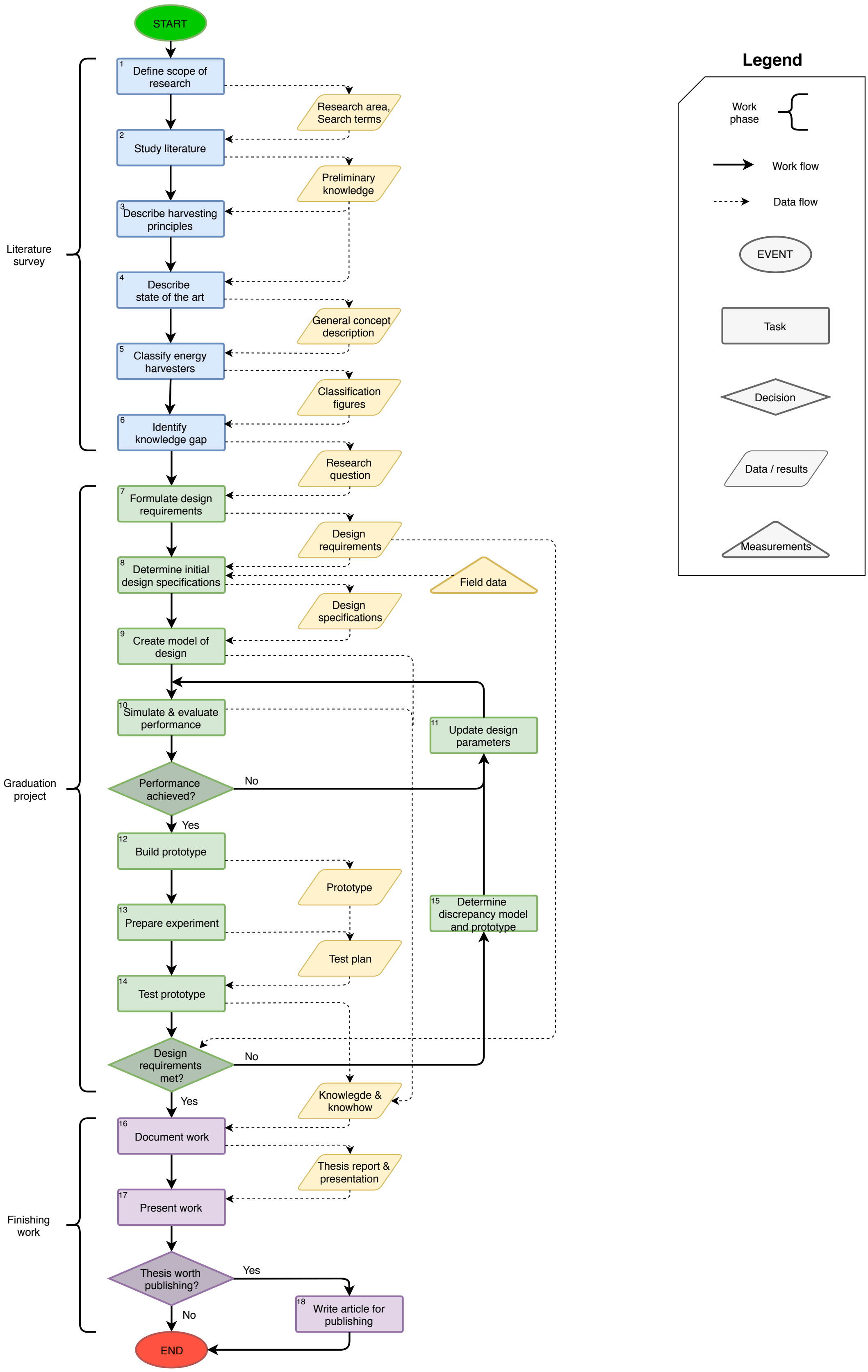

Figure A.1: Workflow diagram of literature study and master's thesis

B
Literature overview

A complete overview of all reviewed papers on vibration energy harvesting in the transportation sector can be found in table B.1.

Table B.1: Overview of papers describing energy harvesting in the transportation sector. Accelerations are given in g's, where 1 g = 1 $m s^{-2}$.

Author	**Year published**	**Times cited**	**Transduction method**	**Application**	**Vibrations analysis?**	**Harvester designed?**	**Harvester tested?**	**Suspension**	**Eigenfrequency** (Hz)	**Acceleration of vibration** (g)	**Output power** (mW)	**Volume** (cm^3)	**Power density** ($mW cm^{-3}$)	**Total mass** (g)
Gatti et al. [28]	2018	0	Piezoelectric	Car (engine)	Yes	Yes	Yes, on shaker	Linear	73; 92; 138	2.5; 4	-	-	13.5	-
Bradai et al. [13]	2018	0	Electromagnetic	Train	Yes	Yes		Linear	29	upto 10	10 (max)	12.3	-	-
Radha et al. [60]	2017	0	Piezoelectric	Vehicles	No	No, only descriptive	No	n/a	n/a	n/a	n/a	n/a	n/a	n/a
Chukwu and Mahajan [18]	2017	0	Piezoelectric	Car	Simulated	No, only modelled	No	Linear	-	-	0.15 (?)	-	-	-
St-John et al. [73]	2016	0	Electromagnetic	Car engine	No	Yes	Yes, sweep on shaker	Non-linear	-	0.5-1.5	-	2.67	-	21.1
Mouapi et al. [51]	2016	3	Piezoelectric	Train	Yes	Yes	Yes, on shaker	Linear	26	0.13	3 (avg)	5.6 (piezo beam)	-	3
Mohamad et al. [49]	2016	0	Piezoelectric	Car	No	No, off the shelf harvester used	Yes, in car	-	-	-	-	-	-	-
Cho et al. [17]	2016	9	Piezoelectric	Train	Yes	Yes	Yes	Non-linear	3.8	0.5	-	0.32 (piezo beam)	0.04	-
Brignole et al. [14]	2016	4	Electromagnetic	Train	Yes	Virtual harvester built	No	Linear	867	1 RMS	50 (peak)	-	-	-
Yeo et al. [86]	2015	2	Electromagnetic	Car, bike	No	Yes, cilindrical	Yes, sweep on shaker	Free	30	-	19 (peak)	95.6	-	150
"	"	"	"	"	"	Yes, donut	"	"	9	-	10 (peak)	95.6	-	150
Mouapi et al. [50]	2015	8	Piezoelectric	Car	Yes	Yes	Yes, in car	Linear	15	∼0.1	0.003 (avg)	Unknown	-	2280
Chan [16]	2014	0	Piezoelectric	Bus	Yes	No, off the shelf harvester used	Yes, in bus	Linear	14	0.0052	0.09	1.02 (piezo beam)	-	38 (tip)
Song et al. [71]	2013	8	Piezoelectric	Train	Yes	Yes	Yes, on shaker	Non-linear	11; 28	-	-	2.4 (piezo beam)	-	-
Orfei et al. [55]	2013	2	Piezoelectric	Automotive	Yes	No, off the shelf harvester used	Yes, on shaker	Non-linear	-	-	1	0.51 (piezo beam)	-	-
Hart et al. [33]	2013	3	Electromagnetic	Train, boat, aircraft	Yes	Yes	Yes, on shaker	Non-linear	10.8	0.45 RMS	1.28 (RMS)	-	-	-
Cueff and Basrour [21]	2013	1	Electromagnetic	Trolley	No	Yes	Yes, on trolley	Free rolling	15	0.05	0.35 (?)	-	0.1	-
Zhu et al. [88]	2012	21	Piezoelectric	Automotive	Yes	Yes	Yes, on car	Linear	17	0.15-1 (max)	0.013 (avg)	-	-	-
Song et al. [70]	2012	5	Piezoelectric	Train	Yes	No, only experimental analysis	No	Linear	70		0.020 (RMS)	-	-	-
Hashimoto et al. [34]	2012	2	Piezoelectric	Car	Yes	Yes	Yes, on shaker	Linear	-	-	-	-	-	-
Dondi et al. [27]	2012	8	Piezoelectric	Vehicle with trailer	Yes	Yes	Yes	Linear	112	0.5-1	0.023-0.85	-	-	-
De Pasquale et al. [26]	2012	29	Electromagnetic	Train	Simulated	No, numerical modelling only	No	Non-linear	4	50 (?)	100	1780	0.056	-
De Pasquale et al. [25]	2012	27	Piezoelectric	Train bogie	Simulated	Yes	Yes, on scale model	Linear	-	0.2	4 (avg)	-	-	-
Scorcioni et al. [68]	2011	6	Piezoelectric	Tractor	Yes	No, off the shelf harvester used	Yes, on shaker	Linear	1000	2	0.5 (avg)	-	-	-
Rahman and Kok [62]	2011	25	n/a	Vehicles, machines, household	Yes	No	No	n/a	n/a	n/a	n/a	n/a	n/a	n/a
Phipps et al. [58]	2011	4	Electromagnetic	Vehicles	Yes	Yes	Yes	Linear	13	0.1	28 (avg)	-	-	-
Baldauf et al. [8]	2011	0	Electromagnetic	Transportation, industrial	Yes	No, only design drawing	No	Linear	12.7	-	0.045 (avg)	-	-	67
Romani et al. [64]	2010	3	Piezoelectric	Train passenger car	Yes	Yes	Yes	Non-linear	-	1.18 RMS	0.04	0.084 (piezo beam)	-	20
Maier et al. [44]	2009	4	Electromagnetic	Train cargo container	Yes	Yes	Yes, on container	Linear	4.5	0.8 RMS	15	-	-	2200

II

Thesis paper

Design of a Vibration Energy Harvester based on Coupled Oscillators

Paulus Schaap, Thijs Blad, Maarten Lustig, Farbod Alijani

***Abstract*—In this paper, the potential benefits of a coupled oscillator electromagnetic vibration energy harvester compared to a single degree of freedom vibration energy harvester is explored. This comparison is made based on the steady-state power output when the harvester is excited at its eigenfrequencies. The harvester concepts are compared based on two cases: one where two frequencies are continuously present, and one where two frequencies are alternately present. These cases are derived from on-road container transport measurements. A single degree of freedom and an array of two single degree of freedom harvesters are used as a benchmark. Three configurations of the coupled oscillator harvester concept are presented, which have been optimized with respect to the magnitude of the electromagnetic damping and the ratio between the two masses. It was found that a coupled harvester with two electromagnetic dampers performs as good as an array of two single degree of freedom harvesters. When using the same proof mass for all concepts, a coupled oscillator harvester with only one electromagnetic damper generates less power than one with two dampers. A prototype has been built to validate the simulations. Good correspondence between simulations and experiments was found, both in terms of output power and optimum electromagnetic damping.**

***Index Terms*—Electromagnetic, multimodal, multi degree of freedom, transportation, container, truck**

I. Introduction

THE current transportation industry market experiences growing demand for wireless sensors in the transportation industry [1, ch.18]. Retailers not only want to track goods to and from their worldwide suppliers but also want to monitor parameters like temperature or acceleration for cooled and fragile products respectively. Other applications may be health monitoring of hard to reach parts in these transportation vehicles. As most often no other power source is available at the location of the measurement device, a so-called ‘vibration energy harvester’ [2] is used to convert mechanical vibrations into electrical energy.

In literature, the most common used transduction methods to convert energy from the mechanical to the electrical domain are piezoelectric energy harvesting [3], [4], electrostatic energy harvesting [5], electromagnetic energy harvesting [6], magnetostrictive energy harvesting [7], [8] or a combination of these methods [9], [10]. In the transport sector, mostly electromagnetic and piezoelectric harvesters are used, having volumes ranging from 0.084 cm^3 [11] to 1780 cm^3 [12] and output power ranging from 3 µW [13] to 50 mW [14]. Various authors have applied different techniques in their harvester design, like a non-linear suspension [12], [15], multimodal harvesting [3], [16] or the use of impacts [17].

However, it does not become clear which harvesting technique is preferred for transport applications. Harvesters proposed in literature have a big range in the energy harvester’s volume, the applied input motion and the output power. On top of that, information required to compare proposed harvesters to others is often not available or presented in a different format. This makes it hard to state what type of harvester would perform the best for transport sector applications.

It is expected that using a multimodal energy harvester will have a higher mean power output from transport applications, as vibrations in this sector normally consist of multiple dominant frequencies in the same direction [18]–[21].

The objective of this research is to explore the potential benefits of a coupled oscillator electromagnetic energy harvester compared to a single degree of freedom (1DoF) harvester. Only two degrees of freedom coupled oscillator will be discussed in this study. The first step into researching the benefits of a coupled oscillator will be comparing them on their most basic behaviour: the steady-state power output when excited at eigenfrequency. The mean output power will be used to compare different harvester concepts. Because the power output will be periodic as the harvester is in steady-state, comparing harvester concepts based on the peak power or root mean square power would give the same relative results.

In the next section, the method used to calculate output power and compare the different energy harvester concepts is described. The results of that comparison are provided in section III. The method and results will be discussed in section IV. This paper ends with conclusions and recommendations in sections V and VI.

II. Method

A. Case description

Because an energy harvester harvests the most energy when excited at its eigenfrequency, a simplified input signal consisting of only two frequencies will be used here. Two cases are created based on these two frequencies.

First, there is the two-tone case having both frequencies present at the same time and the input motion is described by

$$y(t) = Y_1 \sin(\omega_1 t) + Y_2 \sin(\omega_2 t) \tag{1}$$

with Y_i the amplitude of the sine wave in m and ω_i the frequency in $\mathrm{rad\,s^{-1}}$. For this case, the harvester concepts are compared based on their average output power over the total time.

In the second case, the two frequencies are alternatively present, this is the alternating tone case. The input motion is described by

$$y(t) = \begin{cases} Y_1 \sin(\omega_1 t) & \text{for } 0 < t \leq \frac{1}{2}t_\mathrm{t} \\ Y_2 \sin(\omega_2 t) & \text{for } \frac{1}{2}t_\mathrm{t} \leq t \leq t_\mathrm{t} \end{cases} \tag{2}$$

with t_t the total time duration of the signal. In this case, the harvesters will be optimized to have the highest continuous power, so to have maximum power output form both individual frequencies. This means mediocre power output at both frequencies is preferred over a high power output at one frequency but barely any power output at the other. An on-road container transport vibration analysis will be performed to determine the magnitude of frequencies ω_i, of which the results are presented in section III.

If one of the two sine waves from (1) and (2) contains more energy than the other, the most energy can be harvested by tuning a 1DoF harvester to that dominant frequency. To prevent this bias in the optimization procedure, the amplitudes Y_i are chosen such that both sine waves contain an equal amount of power. For this purpose, the amount of power each frequency contains per kilogram is kept constant for both sine waves. This means the magnitude of the input accelerations A_i have to obey the relation

$$\frac{A_1^2}{f_1} = \frac{A_2^2}{f_2} \tag{3}$$

with $A_i = \omega_i^2 Y_i$. A visual representation of the input motion $y(t)$ for both cases obeying (3) is shown in fig. 1.

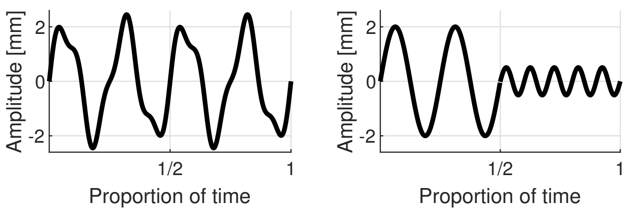

(a) (b)

Fig. 1: The input motion $y(t)$ for the two studied cases: (a) the two-tone case (see (1)) and (b) the alternating tone case with the two frequencies alternatively present, both half of the total time (see (2)).

B. Assumptions

In order to make a fair comparison between different harvester concepts, a few assumptions have been made.

The efficiency of the electrical circuit will not be taken into account as this paper focusses on comparing different harvester concepts based on their mechanical behaviour only.

The total mass is the same for all concepts, as the harvested power scales with the mass of the harvester [22]. A total mass of 0.070 kg will be used as this is the estimated mass of the prototype that will be fabricated to validate the simulations.

The dimensionless parasitic damping ratio is kept the same ($\zeta_\mathrm{p} = 0.014$) for all masses, as the harvested power scales with the parasitic damping. The input motion is not influenced by the motion of the harvester, as the mass of the moving ground is assumed to be a few orders of magnitudes larger than the mass of the harvester.

The electromagnetic damping is assumed to be constant over the period of oscillation. The stiffnesses are also modelled as linear springs, which means the whole harvester is a linear system.

The relation from (3) is set to $\frac{A_i^2}{f_i} = 0.05\ \mathrm{m^2\,s^{-3}}$.

C. Classification of concepts

In this study, five concepts for electromagnetic energy harvesting were considered that can be divided into two groups: the baseline concepts and the coupled oscillator concepts.

1) Baseline concepts: The first concept, concept BH1, is a 1DoF harvester as shown in fig. 2a. The equation of motion for this harvester is described by

$$m\ddot{z}(t) + c_\mathrm{t}\dot{z}(t) + kz(t) = -\ddot{y}(t) \tag{4}$$

with $z(t) = x(t) - y(t)$ the relative motion between the mass and the ground, m the mass of the harvester, k the spring stiffness and $c_\mathrm{t} = c_\mathrm{e} + c_\mathrm{p}$ the total damping ratio with c_e the electromagnetic damping ratio and c_p the parasitic damping ratio defined as [23, ch.2.6]

$$c_\mathrm{p} = 2m\omega_\mathrm{n}\zeta_\mathrm{p} \tag{5}$$

Here, ω_n denotes the harvester's natural frequency in $\mathrm{rad\,s^{-1}}$.

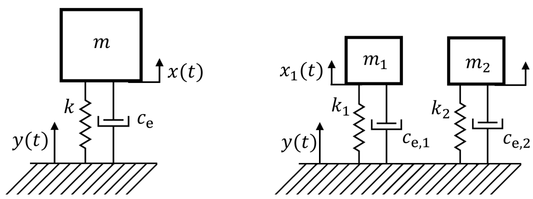

(a) (b)

Fig. 2: Schematic drawings of baseline concepts: (a) a 1DoF harvester (concept BH1) and (b) an array harvester (concept BH2). The conversion of energy from the mechanical into the electrical domain is visualized by an electromagnetic damper c_e. All masses experience parasitic damping as well, but this has been left out of the drawing.

A variation on this is an array of 1DoF harvesters (see fig. 2b), this is concept BH2. The case is considered where each separate oscillator has half the mass of the single 1DoF harvester, i.e. $m_1 = m_2 = \frac{m}{2}$. For $k_1 \neq k_2$ this system has two different eigenfrequencies.

2) Coupled oscillator concepts: Next we have the coupled oscillator harvester concept, of which three variations are considered: electromagnetic damping from the bottom mass only (concept COH1), from the top mass only (concept COH2) or from both masses (concept COH3), see fig. 3.

The equations of motion for the coupled oscillator harvesters

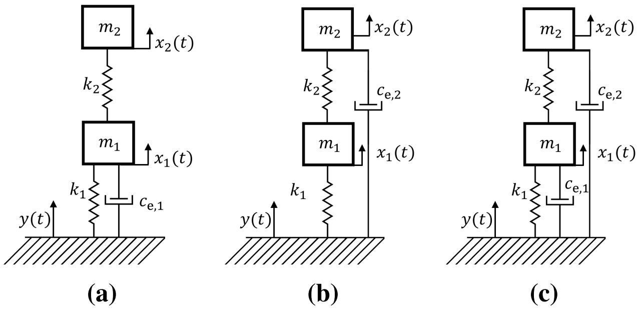

Fig. 3: Schematic drawings of the coupled oscillator harvester. Three different damping configurations are studied, labelled as (a) COH1, (b) COH2 and (c) COH3. All masses experience parasitic damping as well, but this has been left out of the drawing.

in terms of the relative motion between the ground and both masses can be written as

$$\mathbf{M}\ddot{\boldsymbol{z}}(t) + \mathbf{C}_\text{t}\dot{\boldsymbol{z}}(t) + \mathbf{K}\boldsymbol{z}(t) = -\ddot{\boldsymbol{y}}(t) \tag{6}$$

with $\mathbf{M}$, $\mathbf{C}_\text{t}$ and $\mathbf{K}$ the mass, damping and stiffness matrix respectively, $\ddot{\boldsymbol{y}} = \begin{bmatrix}\ddot{y} & \ddot{y}\end{bmatrix}^\intercal$ describing the input acceleration and $\boldsymbol{z} = \begin{bmatrix}z_1 & z_2\end{bmatrix}^\intercal$ the vector of response motion with $z_i = x_i - y$.

The total damping matrix $\mathbf{C}_\text{t}$ is the sum of the parasitic damping matrix and the electrical damping matrix: $\mathbf{C}_\text{t} = \mathbf{C}_\text{e} + \mathbf{C}_\text{p}$. The parasitic damping for this harvester is calculated from the parasitic damping ratio ζ_p as

$$\mathbf{C}_\text{p} = \alpha\mathbf{M} + \beta\mathbf{K} \tag{7}$$

where constants α and β are calculated from $\frac{\alpha}{2\omega_i} + \frac{\beta\omega_i}{2} = \zeta_\text{p}$ [24, p.362].

D. Power comparison procedure

To make a fair comparison between the different harvester concepts, the optimum output power for each concept should be used.

For the 1DoF harvester, the steady-state power P_ss has an optimum for ζ_e. An analytical expression can be derived for the maximum steady-state output power of a 1DoF harvester excited at its eigenfrequency [22]:

$$P_\text{ss} = \frac{m\zeta_\text{e}A^2}{4\omega_\text{n}(\zeta_\text{p}+\zeta_\text{e})^2} = \frac{m\zeta_\text{e}Y^2\omega_\text{n}^3}{4(\zeta_\text{p}+\zeta_\text{e})^2} \tag{8}$$

This formula shows that the maximum power will be harvested when the electromagnetic damping is equal to the parasitic damping, with the remark that this optimum will change a bit when accounting for losses in the electrical circuit [25]. Here the assumption has been made that there is no limit on the stroke and the resulting motion can be achieved. For the array of 1DoF harvesters, the same optimum will be found for each individual oscillator.

For the coupled oscillator harvester, P_ss has an optimum for $\zeta_{\text{e},i}$ and the mass ratio $R_m = \frac{m_1}{m_1+m_2}$. An analytical expression for P_ss in terms of these parameters and the input signal characteristics will give a formula that spans multiple pages and is only valid under various conditions. Due to this complexity, it is difficult to compare the harvesters based on an analytical expression for steady-state power. To still be able to compare the optimum power, an optimization procedure is used to find the maximum power for a coupled oscillator harvester.

When optimizing for the two-tone case, the objective function of the optimizer is to maximize the average power output over the total time, which is the sum of the power harvested from both individual frequencies:

$$P_\text{avg} = P_{\omega_1} + P_{\omega_2} \tag{9}$$

with P_t the total harvested power and P_{ω_i} the power harvested from each individual frequency. As the system is assumed linear, the power harvested from these two signals can be calculated separately and then be added up, see section II-B. This is done using the the superposition theorem, which can be applied when the system is assumed linear [26, ch.18.1].

When optimizing for the alternating tone case, the goal was to harvest the maximum continuous power. The average power over the total time is calculated as

$$P_\text{avg} = \tfrac{1}{2}P_{\omega_1} + \tfrac{1}{2}P_{\omega_2} \tag{10}$$

It is important that the optimizer converges to a point where the power harvested from both frequencies is maximized. For this reason, a threshold has been applied for the power harvested from both individual frequencies. The optimizer then finds an optimum in the area bound by the two applied threshold values. The power threshold is gradually increased in the optimization process until the area bounded by these boundaries becomes negative, i.e. there are no points in the P_t optimization area that meet both P_{ω_i} thresholds.

E. Optimization of coupled oscillator harvester

An optimization procedure is used to maximize the coupled oscillator harvester in terms of steady-state output power. The found optimum can then be compared with the optimum power from a 1DoF harvester from (8). The optimization parameters are these for which the steady-state power P_ss has an optimum. These are the electrical damping coefficient(s) $c_{\text{e},i}$ and the mass ratio $R_m = \frac{m_1}{m_1+m_2}$. The harvester's eigenfrequencies will be tuned to the frequencies of the input signal.

The optimizer calculates the steady-state output power while varying the optimization parameters $c_{\text{e},i}$ and R_m. In this procedure, the optimizer uses the solution for the steady-state motion as function of the optimization parameters to calculate the output power. This steady-state solution can be calculated from (6) via the method of undetermined coefficients [27, ch.4].

Energy harvested during one period of the input oscillation can now be calculated as

$$E_T = \int_0^T c_{\text{e},1}\dot{x}_1^2 \mathrm{d}t + \int_0^T c_{\text{e},2}\dot{x}_2^2 \mathrm{d}t \tag{11}$$

with $T = \frac{1}{f_\text{input}}$ the period of the input frequency and nDoF the number of degrees of freedom of the oscillator. If a two DoF harvester is used with only one electromagnetic damper (i.e. the harvesters from figs. 3a and 3b), $c_{e,i}$ will be zero for the damper that is not present. The average harvested steady-state power can now be calculated as

$$P_{ss} = \frac{E_T}{T} \tag{12}$$

A few constraints are imposed on the optimization process to bound the optimization procedure. To prevent the coupled oscillator harvester from converging to a 1DoF harvester, the mass ratio is constrained to the interval [20%, 80%].
Because the amplitudes of both masses for the assumed ζ_p are negligible compared to the dimensions of the harvester, no constraint is applied to bound these amplitudes.
During the optimization procedure, the ratio between the top and bottom mass is varied. To keep the eigenfrequencies of the harvester the same (they should still match the frequencies of the input signal regardless of the mass ratio), the stiffnesses should change when varying the mass ratio. For each mass ratio the stiffness is calculated from the relation between the mass and stiffness matrix and the eigenfrequencies of the coupled oscillator:

$$\left|\mathbf{K} - \omega_i^2 \mathbf{M}\right| = \left|\begin{bmatrix} k_1 + k_2 & -k_2 \\ -k_2 & k_2 \end{bmatrix} - \omega_i^2 \begin{bmatrix} m_1 & 0 \\ 0 & m_2 \end{bmatrix}\right| = 0 \tag{13}$$

From this relation it follows that the minimum possible mass ratio is constrained by

$$R_m = \frac{4R_f^2}{R_f^4 + 2R_f^2 + 1} \tag{14}$$

with $R_f = \frac{f2}{f1}$ the frequency ratio. With a maximum mass ratio constraint of 80%, the minimum frequency ratio would be 1.6. As the smallest frequency ratio for the cases described in section II-A is $R_f = \frac{50}{20} = 2.5$, this constraint will not be violated.

F. Realization of prototype

A coupled oscillator prototype have been built in order to validate the results from the simulations by means of experiments. The 1DoF harvester can be tested by fixing the first mass of the coupled oscillator, after which the second mass will act as a 1DoF harvester.
Laser cut acrylic sheet was used for structural elements. Masses were suspended by means of steel leaf springs that were fixed with super glue in dedicated cut-out slots, see fig. 4a. The used magnet set generates a magnetic field of $B = 0.82$ T. The used coil has $N = 2900$ windings, an effective width of $w = 0.025$ m and a resistance of $R_{coil} = 275$ Ω. For the used coil, the impedance can be neglected with respect to the coil resistance. The applied electromagnetic damping can be calculated as [28]

$$c_e = \frac{(NBw)^2}{R_{load} + R_{coil} + Z_{coil}} \tag{15}$$

with R_{load} the resistance of the connected load in Ω and Z_{coil} the coil impedance in Ω. The amount of electromagnetic damping can be changed by tuning the load resistance R_{load}. The prototype was designed to have eigenfrequencies 20 & 50 Hz. 3D finite element modelling software was used to determine out-of-plane eigenfrequencies. The prototype was designed such that it had no out-of-plane eigenfrequencies under 100 Hz, as eigenfrequencies close to the harvesting frequencies will disturb the measurements. The prototype harvester has dimensions $155 \times 34 \times 90$ mm and weights 0.64 kg. The mass of the first and second oscillator are 0.028 and 0.030 kg respectively.

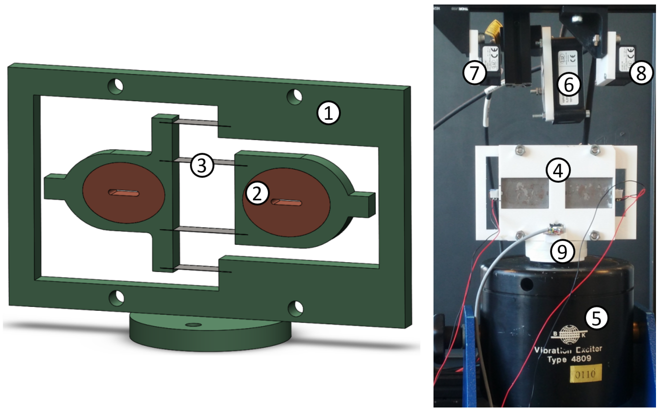

(a) (b)

Fig. 4: Coupled oscillator prototype. (a) shows a 3D CAD drawing of the harvester without magnets, showing ① acrylic sheet, ② coils and ③ leaf springs. (b) shows the test setup consisting of ④ prototype on ⑤ vibration generator with ⑥⑦⑧ lasers measuring positions of ground and both moving masses and an ⑨ accelerometer measuring the input accelerations.

G. Experimental setup

The prototype's exact eigenfrequencies are measured by doing an FFT analysis on the vibrations recorded after giving an impact on the harvester.
To validate the parasitic damping assumption made in section II-B the parasitic damping of the prototypes will have to be measured. For the 1DoF prototype, this will be done using the logarithmic decrement method [23, ch.2.6.3]. As no methods to experimentally determine the parasitic damping for a coupled oscillator were found, the measured parasitic damping from the 1DoF prototype will be applied to the masses of the coupled oscillator as well.
To calculate the parasitic damping, the 1DoF prototype is fixed to a heavy granite table. The mass is given an initial displacement, after which the rate of decay over the measured voltage over R_{load} was measured to calculate the damping ratio. R_{load} can now be plotted against the Q-factor defined as $Q = \frac{1}{2\zeta}$ [23, p.276]. The theoretical Q-factor will be based on the measured parasitic damping, and is calculated by using (15). A fit through the data points will be made by shifting the theoretical curve.
When connecting a very large load resistance, the current that

flows through the resistor can be neglected and it can be assumed that there is no electromagnetic damping. The measured damping for this R_{load} will be the parasitic damping.

To test the prototype during operation, it will be mounted on a vibration exciter. Both the accelerations and displacements of the input are measured. From the oscillating masses, only the displacements are measured. See fig. 4b.
The measured positions and accelerations are not fed back to the input source. The user is, however, able to manually adjust the input after reading out the measurement data. This way the input vibrations are constrained such that the amplitude of the oscillator is smaller than 5% of the flexure length. Doing so, non-linear spring behaviour is kept to a minimum.
Only single-frequency input vibrations will be used during the experiments.
The power dissipated over the load resistance when exciting the harvester is measured using Joule's law and Ohm's law:

$$P_{\text{load}} = \frac{U^2}{R_{\text{load}}} \tag{16}$$

with U the voltage drop over the load. During the measurements, the voltage going into the vibration exciter will be kept constant.
To avoid the effect of variations in input motion, the generator figure of merit (FoM_G) [29] will be calculated for each measurement. The density of the proof mass is set equal to the density of copper, which gives $\rho_M = 8.96 \cdot 10^3\ \text{kg}\,\text{m}^{-3}$ [30]. The FoM_G will be calculated based on the measured accelerations.

III. Results

A. Case study

Measurements on the on-road container transport show that the vibrations are uniform along the container and are invariant with respect to the speed of the truck. The most dominant frequencies were found to be at 20, 50, 80 and 160 Hz, with 20 Hz being the most present. In the cases from section II-A, ω_1 will be set to 20 Hz and ω_2 will be one of the other three frequencies.

B. Simulated power baseline harvesters

The maximum harvestable steady-state output power from the 1DoF harvester for the two-tone case can be calculated by filling in (8) for $\zeta_e = \zeta_p$, which gives $P_{ss} = 2.5$ mW. The power for the array harvester will be 1.25 mW for each individual oscillator, which gives a total P_{ss} of 2.5 mW as well. For the alternating tone case, where the two frequencies are alternatively present, the 1DoF harvester will be able to harvest only from one of the two frequencies, which gives an average of 1.25 mW over the total time, see fig. 5. The array harvester will harvest 1.25 mW from both frequencies, which also gives an average of 1.25 mW.
From (8) it can be concluded that the results presented in this section can be extrapolated linearly for larger masses or higher input accelerations, provided that the assumptions made in section II-B are still met and the system remains linear.

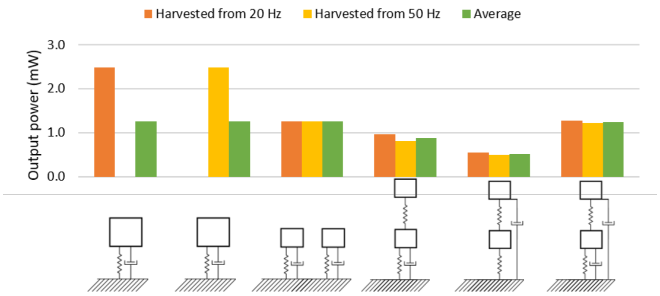

Fig. 5: Simulated harvested power for the alternating tone case. The 1DoF harvester appears twice, as it can be tuned to either 20 or 50 Hz. Coupled oscillator harvesters were optimized to have the output power from both frequencies as equal as possible.

C. Simulated power coupled oscillator harvesters

Fig. 6a shows the optimization plot when COH1 is excited at its first eigenfrequency. Fig. 6b shows the plot when this harvester is excited at its second eigenfrequency. The optimal electromagnetic damping was found to shift when the frequencies of the input signal change, i.e. the optima shift along the x-axis in figs. 6a and 6b.

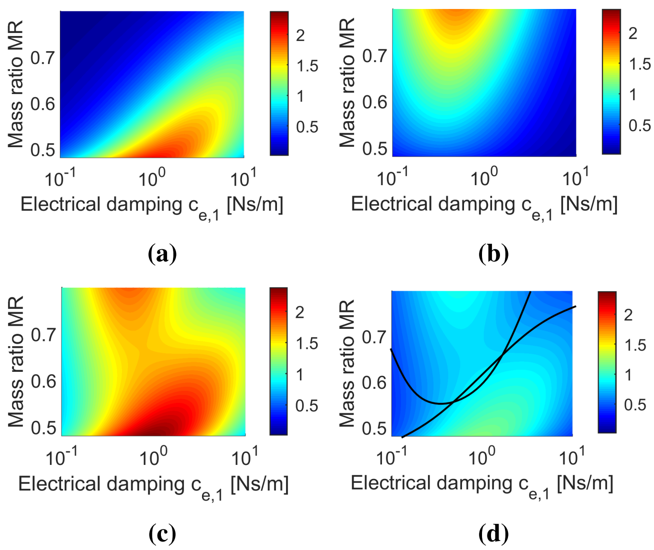

Fig. 6: Example of output power [mW] optimization landscape for coupled oscillator with bottom damper only: (a) power harvested from 20 Hz signal, (b) from 50 Hz signal, (c) from 20 & 50 Hz at the same time (two-tone case) and (d) from 20 & 50 Hz alternating (alternating tone case) with a threshold of 0.8 mW (black lines). The mass ratio is bound by (14) which gives a minimum possible mass ratio of $R_m \approx 0.48$.

For the two-tone case, the total power is calculated according

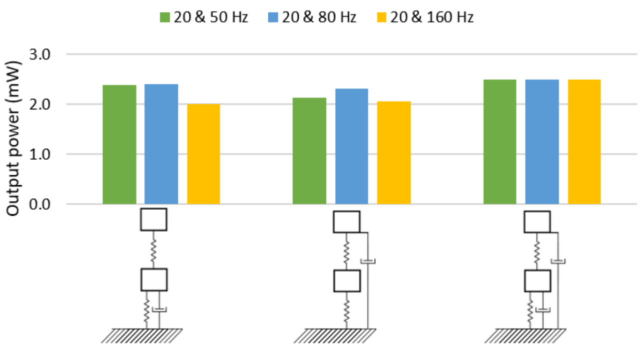

Fig. 7: Simulated harvested power for the two-tone case. Only the coupled oscillators are compared here, the 1DoF and array harvester both provide 2.5 mW in all three situations.

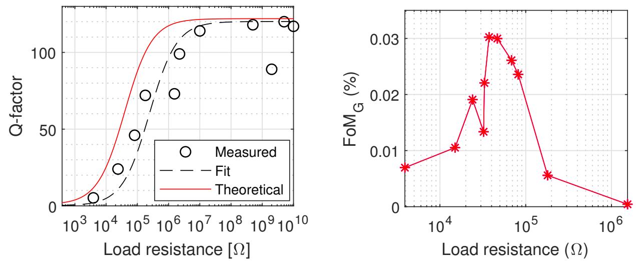

(a) **(b)**

Fig. 8: Response of 1DoF harvester prototype: load resistance R_{load} versus (a) measured Q-factor after oscillator impact and (b) average measured output power over maximum harvestable power when excited at eigenfrequency.

to (9), resulting in fig. 6c. The optimization landscape is saddle shaped, with the optimum belonging to the first eigenfrequency being the global optimum. In fig. 7 the output power for the coupled oscillator harvesters when subjected to the input signal from the two-tone case are compared. It was found that for $R_f \approx 4$ the two optima from fig. 6c line up, which gives the highest total power output compared to other frequency ratios where the two optima are further apart on the x-axis.
For the alternating tone case, the total power is calculated using (10). Here the same saddle shaped landscape was found, but with a lower magnitude. The optimization landscape together with the power thresholds of 0.8 mW are plotted in fig. 6d. As most power is harvested from the first eigenfrequency, the optimizer converges to a point as close to the optimum for the two-tone case as allowed by the threshold power constraint. Fig. 5 compares the output power of different harvesters for the alternating tone case. The total average output power of the COH1 is 30% less than that of the array harvester. For COH2 this is 60%. COH3 has the same total average output power as the array harvester. Only the case where $w_2 = 50$ Hz is plotted in fig. 7. It was found that for higher frequency ratios (i.e. higher w_2), the power harvested from the second frequency decreases even more. This means the parabolic threshold line from fig. 6d shifts upwards, resulting in a lower maximum threshold value that can be applied. For $w_2 = 80$ Hz and $w_2 = 160$ Hz no optimum was found for a threshold larger than 0.5 mW.

D. Prototype characterisation

It was found that the 1DoF prototype had an eigenfrequency of 23.30 Hz. The eigenfrequencies of the coupled oscillator prototype were found as 19.17 and 47.61 Hz.
In fig. 8b, R_{load} is plotted versus the measured Q-factor. A maximum Q-factor of 120 was found. This means the parasitic damping ratio in the prototype is $\zeta_{\text{p}} = 0.0042$, which corresponds to a parasitic damping coefficient of $c_{\text{p}} = 0.037$ $\text{N}\,\text{s}\,\text{m}^{-1}$.

E. Experimental power output

When measuring the shaker accelerations when exciting the prototype, it was found that there were higher orders of the desired input frequency present. The magnitude of these higher order frequencies was approximately fifty times lower than the magnitude of the desired input frequency.
In figs. 8b and 9 the FoM$_G$ is plotted against R_{load}. For the 1DoF harvester a maximum FoM$_G$ of 0.03% was found. The COH1 had a maximum FoM$_G$ of 0.035% when excited at its first eigenfrequency, and 0.0062% when excited at its second eigenfrequency. For the COH2 this was 0.038% and 0.011% respectively.

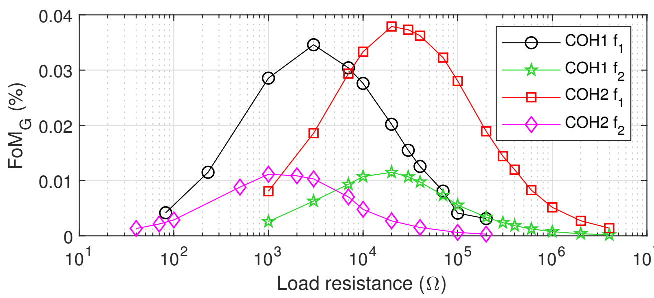

Fig. 9: Generator figure of merit based on measured power output for different R_{load}. f_i denotes the coupled oscillator harvesters being excited at their ith eigenfrequency.

IV. Discussion

A. Discussion of method

1) Simulation method: In this research the power per mass present in both frequencies was set equal. In reality, this will most likely not be the case, and one frequency will always contain more power than the others. To still be able to harvest an equal amount of power from both frequencies in the alternating tone case, the harvester should be tuned more towards the frequency containing less power per kilogram.
As the harvester concepts are only compared in terms of their steady-state output power, these results are only applicable

to situations where the dominant frequencies are present long enough so that the harvester can reach steady-state. For signals with rapidly changing frequencies, it matters more how fast the harvester can start up, instead of what its steady-state power is. For such signals, a comparison in harvester transient behaviour is needed rather than a steady-state power comparison.

In this research, a simplified signal is used with only two frequencies. This will most probably not occur in practice, and other frequencies will always be present. Frequencies close to the eigenfrequency of the harvester could contribute to the total output power as well, but the effect of this on the comparison between 1DoF and coupled oscillator harvesters has not been studied here.

2) Experimental method: Only the electromagnetic damping was varied during experiments. The optimum mass ratio for the coupled oscillator harvester has not been validated. What makes the procedure of validating the mass ratio difficult is the fact that the springs are not replaceable, and thus the harvester's eigenfrequencies will change after changing the mass ratio. This harvester with different eigenfrequencies will have a different electromagnetic damping optimum as well, which makes the experimental optimization process cumbersome.

During the experiments, the power harvested from both individual eigenfrequencies is measured, but no response to dual frequency input vibration was tested. This means the assumption that the system is completely linear, so its response to a multi-frequency input can be obtained by adding the response of each individual response to a single frequency input, has not been validated.

B. Discussion of results

1) Simulation results: Based on simulations, a 1DoF harvester gives the highest output power for the two-tone case. This can be explained as follows: as both frequencies are continuously present, and they both contain the same amount of power per mass, it does not matter from which one you harvest, or if you harvest from both. This also becomes clear when looking at the optimization plots: the coupled oscillator converges to a very high or very low mass ratio. It actually wants to converge to a 1DoF system, which indicates this is the preferred harvester for this case.

Contrary to the hypothesis made in section I, the coupled oscillator harvester is not able to harvest more energy from a vibration signal with alternating frequencies (the alternating tone case). The reason for this is that there are two local optima in the optimization landscape, with each optimum belonging to one input frequency. This means a trade-off has to be made how much the coupled oscillator harvests from each frequency.

The fact that two of the three coupled oscillator harvester concepts only need one damper instead of two when using the array harvester is an advantage of the coupled oscillator. The assumption has been made that the design space is completely filled with the moving mass. In practice, however, creating an electromagnetic damper will require some design space as well. When only one electromagnetic damper is needed instead of two, more design space can be dedicated to the moving mass. As power scales linear with the harvester's mass, this will increase the performance of a coupled oscillator harvester with one damper.

A disadvantage of the coupled oscillator harvester is that, in the alternating tone case, it only performed well for eigenfrequencies 20 & 50 Hz. Increasing the second eigenfrequency led to a lower power output. This would argue that the coupled oscillator harvester is most profitable when its eigenfrequencies are closer together. This is however only possible to a certain extent, as the constraint from (14) will limit the mass ratio when the frequencies get closer together.

A small sensitivity analysis is performed to check if the mass ratio is sensitive to variations in parasitic damping. It was found that there was a decrease of 2% in R_m when the parasitic damping was changed from 1.4% to 5.4%.

2) Experimental results: Because the shaker has a suspension with a certain stiffness as well, the shaker adds a degree of freedom to the system. The motion of the shaker is thus influenced by the motion of the oscillators, and antiresonance peaks occur.

From (8) it followed that the maximum power from the 1DoF prototype is harvested when the electromagnetic and parasitic damping are equal. Looking at fig. 8a, this would mean maximum power would be harvested from the 1DoF harvester for $R_{\text{load}} \approx 180$ kΩ. During experiments, most power was harvested for $R_{\text{load}} \approx 37$ kΩ, see fig. 8b. Table I gives an overview of the experimentally found optimum load resistance from fig. 9 and the corresponding electromagnetic damping calculated from (15). These values are compared to the theoretical optimum found in a similar method as the results from section III, but now with the measured parasitic damping of $\zeta_{\text{p}} = 0.0042$ as an input.

TABLE I: Comparison of theoretical optimal and experimentally determined optimal electromagnetic damping. f_i denotes the coupled oscillator harvesters being excited at their ith eigenfrequency.

	Exp. opt. R_{load} [kΩ]	Corresp. c_{e} [N s m^{-1}]	Theor. opt. c_{e} [N s m^{-1}]
1DoF	37	0.055	0.031
COH1 f_1	30	0.068	0.28
COH1 f_2	200	0.010	0.085
COH2 f_1	200	0.010	0.038
COH2 f_2	1	1.6	0.90

A discrepancy of approximately 50% was found between the theoretical and experimental optimum c_{e}. In [31] and [32] experiments on an electromagnetic energy harvester are done as well. Here, also a small discrepancy between theoretical and experimental optimum R_{load} was found. In [32] it was stated that the main cause for this difference in found optima is the existence of a back electromotive force when current passes through the coils. As the current through the coil is less than 50 mA in the cases tested in this work, it is not plausible that this is the reason for the discrepancy in this work. What is more likely is that some of the parameters used in (15) are not entirely correct. As the numerator is squared in this formula, the error in resulting electromagnetic damping grows fast. Most probably the magnetic field is not exactly as simulated, which causes a different ΔB. Also, the effective width of the coil w might differ a bit from the estimations because of the coil's oval shape.

C. Reflection on prior art

In contrast to the multimodal harvesters proposed by e.g. [3], [16], [33] to harvest from multi-frequency transport applications, this work has tried to optimize and compare a particular type of multimodal harvester. Making such a comparison is insightful, as it shows if the proposed design is indeed preferred over a simple 1DoF harvester.
Results from simulations and experiments are presented in a way that makes it easy to compare the studied harvesters with other energy harvesting concepts that were not considered in this work. By calculating the generator figure of merit, it is easy to compare these harvesters with others.
When adding the harvesters from this paper to the FoM_G overview from [29], they are positioned in the lower region of figure 5. A reason why our prototypes perform worse than most others in this comparison, is the fact that the prototypes are not optimized for their total dimensions.

V. Conclusions

Three configurations of a coupled oscillator harvester have been compared to a 1DoF harvester and an array of two 1DoF harvesters. The comparison is based on two cases: a two-tone and alternating tone case.
It was found that if the two dominant frequencies in a signal are continuously present like in the two-tone case, a 1DoF harvester is the best option. During the optimization, the coupled oscillator converged to a 1DoF oscillator.
When the two dominant frequencies are alternatively present like in the alternating tone case, the 1DoF harvester can only harvest from one of the two frequencies. Having a harvester that can harvest from both frequencies will be beneficial when continuous power output is required. It was found that the coupled oscillator harvester with two electromagnetic dampers had the same total average output power as the array harvester. The total average output power of coupled oscillators with one electromagnetic damper is 30 to 60% less than that of the array harvester.

The practical benefit of two of the coupled oscillator concepts is that they only require one electromagnetic damper, which means their moving mass could be a bit heavier in practice and thus harvest more power than a harvester that needs two electromagnetic dampers.

In experiments the found electromagnetic damping was varied and an optimum was found for output power. The COH1 and COH2 were tested at both their eigenfrequencies. The optimum electromagnetic damping determined from experiments deviated approximately 50% from the theoretical optima.

VI. Recommendations

Based on steady-state power output in multi-frequency environments, it is recommended to design an array of 1DoF harvesters. For environments with quickly alternating dominant frequencies, this work is not able to give an adequate recommendation. For this situation, research into transient behaviour and off-eigenfrequency excitation of different harvester concepts is recommended.
The experiments performed in this work show that a prototype on an experimental setup can behave a little different than predicted with a computer model. It is recommended to do a more extensive experimental study, or even start with an experimental study in future research. Testing harvester prototypes with a dual frequency input will give better insight in the harvester's response to the two-tone case. It will also help to validate the assumption that the power harvested from a multi-frequency input can be calculated by adding the harvested power from both frequencies individually. This will provide practical and applicable knowledge from the start of the research. Also, experiments with a multi-frequency input are recommended, which have not been done in this study.
When doing measurements, it is strongly recommended to use a closed loop setup, i.e. control the input motion with a computer based on real-time measurements like done in [12], [34]. This will make it possible to make an absolute comparison between different concepts instead of having to correct for different input conditions. Also the added dynamics because of the dynamics of the shaker are avoided. As the used shaker generated higher orders of the desired frequency as well, it is advised to use prototypes of which the second eigenfrequency is not a multiple of the first one.

References

[1] S. Priya and D. J. Inman, *Energy harvesting technologies*. Springer, 2009.

[2] C. B. Williams and R. B. Yates, "Analysis of a micro-electric generator for microsystems," *SENSORS AND ACTUATORS A*, vol. 52, no. 1/3, pp. 8–11, 1996.

[3] C. Gatti, J. Ramirez, M. Febbo, and S. Machado, "Multimodal piezoelectric device for energy harvesting from engine vibration," *Journal of Mechanics of Materials and Structures*, vol. 13, no. 1, pp. 17–34, 2018.

[4] G. De Pasquale, A. Som, and F. Fraccarollo, "Piezoelectric energy harvesting for autonomous sensors network on safety-improved railway vehicles," *Proceedings of the Institution of Mechanical Engineers, Part C: Journal of Mechanical Engineering Science*, vol. 226, no. 4, pp. 1107–1117, 2012.

[5] C. P. Le, E. Halvorsen, O. Sorasen, and E. M. Yeatman, "Microscale electrostatic energy harvester using internal impacts," *Journal of Intelligent Material Systems and Structures*, vol. 23, no. 13, pp. 1409–1421, 2012.

[6] D. Spreemann and Y. Manoli, *Electromagnetic Vibration Energy Harvesting Devices*. Springer, 2012.

[7] K. Chomsuwan, N. Srisuthep, C. Pichitronnachai, and U. Toshiyuki, "Energy free railway monitoring with vibrating magnetostrictive sensor for wireless network sensor," in *2017 Eleventh International Conference on Sensing Technology (ICST)*, Conference Proceedings, pp. 1–5.

[8] L. Wang and F. G. Yuan, "Vibration energy harvesting by magnetostrictive material," *Smart Materials and Structures*, vol. 17, no. 4, 2008.

[9] Y. Tadesse, Z. Shujun, and S. Priya, "Multimodal energy harvesting system: Piezoelectric and electromagnetic," *Journal of Intelligent Material Systems and Structures*, vol. 20, no. 5, pp. 625–632, 2009.

[10] R. C. Vinod, M. G. Prasad, and T. F. Frank, "A coupled piezoelectric-electromagnetic energy harvesting technique for achieving increased power output through damping matching," *Smart Materials and Structures*, vol. 18, no. 9, 2009.

[11] A. Romani, C. Tamburini, A. Golfarelli, R. Codeluppi, M. Dini, E. Sangiorgi, M. Tartagni, and R. Paganelli, *Actively controlled power conversion techniques for piezoelectric energy harvesting applications*. Dordrecht: Springer, 2010, vol. 54, pp. 359–363.

[12] G. De Pasquale, A. Som, and N. Zampieri, "Design, simulation, and testing of energy harvesters with magnetic suspensions for the generation of electricity from freight train vibrations," *Journal of Computational and Nonlinear Dynamics*, vol. 7, no. 4, 2012.

[13] A. Mouapi, N. Hakem, G. Y. Delisle, and N. Kandil, "A novel piezoelectric micro-generator to power wireless sensors networks in vehicles," in *2015 IEEE 15th International Conference on Environment and Electrical Engineering (EEEIC)*, 2015, Conference Proceedings, pp. 1089–1092.

[14] O. Brignole, C. Cavalletti, A. Maresca, N. Mazzino, M. Balato, A. Buonomo, L. Costanzo, M. Giorgio, R. Langella, A. L. Schiavo, A. Testa, and M. Vitelli, "Resonant electromagnetic vibration harvesters feeding sensor nodes for real-time diagnostics and monitoring in railway vehicles for goods transportation: A numerical-experimental analysis," 2016, Conference Proceedings, pp. 456–461.

[15] J. St-John, P. Alevras, S. Theodossiades, H. Rahnejat, and P. Kelly, "Nonlinear energy harvesting from base excitation in automotive applications," 2016.

[16] S. Hashimoto, N. Nagai, Y. Fujikura, J. Takahashi, S. Kumagai, M. Kasai, K. Suto, and H. Okada, "Development of a power generation device for multi-mode vibration in automobiles," in *The 2012 International Conference on Advanced Mechatronic Systems*, 2012, Conference Proceedings, pp. 134–138.

[17] D. Song, H. Jang, S. B. Kim, and T. H. Sung, "Piezoelectric energy harvesting system for the vertical vibration of superconducting maglev train," *Journal of Electroceramics*, vol. 31, no. 1-2, pp. 35–41, 2013.

[18] J. Y. Cho, S. Jeong, H. Jabbar, Y. Song, J. H. Ahn, J. H. Kim, H. J. Jung, H. H. Yoo, and T. H. Sung, "Piezoelectric energy harvesting system with magnetic pendulum movement for self-powered safety sensor of trains," *Sensors and Actuators, A: Physical*, vol. 250, pp. 210–218, 2016.

[19] A. Mouapi, N. Hakem, N. Kandil, and G. V. Kamani, "Energy harvesting design for autonomous wireless sensors network applied to trains," vol. 2016-November, 2016, Conference Proceedings.

[20] Q. Zhu, M. Guan, and Y. He, "Vibration energy harvesting in automobiles to power wireless sensors," in *2012 IEEE International Conference on Information and Automation*, 2012, Conference Proceedings, pp. 349–354.

[21] F. Maier, M. Sturmlechner, and S. Dierneder, "Novel energy harvester with low friction losses," in *Systems, Signals and Devices, 2009. SSD'09. 6th International Multi-Conference on*. IEEE, 2009, Conference Proceedings, pp. 1–6.

[22] S. P. Beeby, M. J. Tudor, and N. M. White, "Energy harvesting vibration sources for microsystems applications," *Measurement Science and Technology*, vol. 17, no. 12, p. R175, 2006.

[23] S. S. Rao, *Mechanical Vibrations*, 5th ed. New York: Pearson Education Inc., 2011.

[24] D. J. Inman, *Engineering Vibrations*, 4th ed. New Jersey: Pearson Education Inc., 2014.

[25] N. G. Stephen, "On energy harvesting from ambient vibration," *Journal of Sound and Vibration*, vol. 293, no. 1, pp. 409–425, 2006.

[26] R. A. Serway and J. W. Jewett, *Physics for Scientists and Engineers with Modern Physics*, 9th ed. Cengage Learning Inc, 2013.

[27] R. K. Nagle, E. B. Saff, and A. D. Snider, *Fundamentals of Differential Equations*, 8th ed. Addison-Wesley, 2012.

[28] M. El-hami, P. Glynne-Jones, N. M. White, M. Hill, S. Beeby, E. James, A. D. Brown, and J. N. Ross, "Design and fabrication of a new vibration-based electromechanical power generator," *Sensors and Actuators A: Physical*, vol. 92, no. 1, pp. 335–342, 2001.

[29] T. W. A. Blad and N. Tolou, "On the efficiency of energy harvesters: a classification of dynamics in miniaturized generators under low-frequency excitation." *SAGE Publications*, 2018.

[30] CES EduPack 2018. Granta Design.

[31] C. R. Saha, T. O'Donnell, H. Loder, S. Beeby, and J. Tudor, "Optimization of an electromagnetic energy harvesting device," *IEEE Transactions on Magnetics*, vol. 42, no. 10, pp. 3509–3511, 2006.

[32] B. Yang, C. Lee, W. Xiang, J. Xie, J. H. He, R. K. Kotlanka, S. P. Low, and H. Feng, "Electromagnetic energy harvesting from vibrations of multiple frequencies," *Journal of Micromechanics and Microengineering*, vol. 19, no. 3, p. 035001, 2009.

[33] M. Cueff and S. Basrour, "A multi degree of freedom vibration magnetic energy harvester for transport application," in *Journal of Physics: Conference Series*, vol. 476. IOP Publishing, 2017, Conference Proceedings, p. 012092.

[34] A. Rahimi, O. Zorlu, A. Muhtaroglu, and H. Kulah, "Fully self-powered electromagnetic energy harvesting system with highly efficient dual rail output," *IEEE Sensors Journal*, vol. 12, no. 6, pp. 2287–2298, 2012.

III

Appendices

In appendix A.2 the procedure of doing measurements on a container transportation truck is described. Appendix B shows the calculations behind the mass ratio constraint as a function of the frequency ratio defined in part II. In appendix D.3.3 more detailed information regarding the calculations, fabrication and experimental testing of the prototype are explained.

A
Case description

As described in the literature review chapter 1, there is a growing demand for wireless sensors in the transportation industry. One common way of transporting goods is by means of intermodal containers. As a lot of intermodal containers are transported by road on container trucks, Kinergizer B.V. experiences a growing demand for harvesting energy from container vibrations on trucks. To meet this market demand, the case of harvesting electrical energy from containers being transported on trucks is being investigated in this research.

A.1. Vibration measurement setup

To get some idea of the nature of the vibrations present in a container transported on a truck, measurements have been performed on a container that was transported between two terminals in the harbour of Rotterdam (see fig. A.2). The truck used was a Scania R410 in combination with a Tracon Trailers semi-trailer, both owned by Van Tiel Transport B.V. Rotterdam. A 20 feet long container weighting approximately 30 tonnes was loaded on the semi-trailer.

Figure A.1: Picture of the container mounted on the truck on which the measurements are performed. The zoomed part shows the SlamStick measuring device taped to the container. Extra tape was added to create a better connection after the picture was taken. Picture taken at Maasvlakte.

To measure the vibrations in the container, two vibration measurement devices were mounted on the container. The advantages of using two accelerometers is that the vibrations at multiple positions on the container can be recorded, and that there is always a backup measurement device in case one of the devices fails. Another benefit of using two different accelerometers is that measurement errors caused by the measurement device itself can be pinpointed by comparing the results from both accelerometers. In this case, although the devices are mounted very rigidly to the container, there still is the possibility of signal pollution because the

Figure A.2: The route driven by the truck carrying the container on which the measurements were performed. The first ride was from Rotterdam (green marker) to the Maasvlakte (red marker), the second one was from the Maasvlakte back to Rotterdam. Map ©Google Inc.

mounted measurement device is vibrating relatively to the container. Because the different accelerometers used have different masses, the frequencies of these vibrations should be different if they are present at all.
The first device was a MIDE Slam Stick X triaxial accelerometer [**?**]. The second device was an Axivity 3-axis logging accelerometer [**?**]. After wiping off the dust and small debris stuck to the container, the accelerometers were attached to the container by means of ultra thin double sided tape. This created a very rigid connection between the accelerometer and the container. Ultra thin tape was used to reduce the damping of vibrations in the accelerometer due to the tape layer to a minimum. After taping the accelerometer to the container, extra single sided tape was put over the accelerometers to fixate them even better. Both accelerometers were set to measure at their maximum sample rate, i.e. 10 kHz for the MIDE Slam Stick and 3.2 kHz for the Axivity AX3 device. Vibrations in all three directions have been recorded.
During the first ride the MIDE Slam Stick X was mounted on one of the doors at the rear side of the container, while the Axivity AX3 was mounted in the middle of the left side of the container. During the second ride both accelerometers were mounted on the left side of the container: the Axivity AX3 more to the front and the MIDE Slam Stick X more to the rear of the left side (see fig. A.1).

A.2. Vibration measurement results

Figure A.3 gives an example of the vibration spectrum measured on the truck. From the different measurements it could be concluded that the same dominant frequencies were present in the whole container, i.e. the waterfall diagrams from different measurements were very similar. From fig. A.3 the dominant frequencies at 20, 50 and 80 Hz are clearly visible, which the cases in part II are based on.

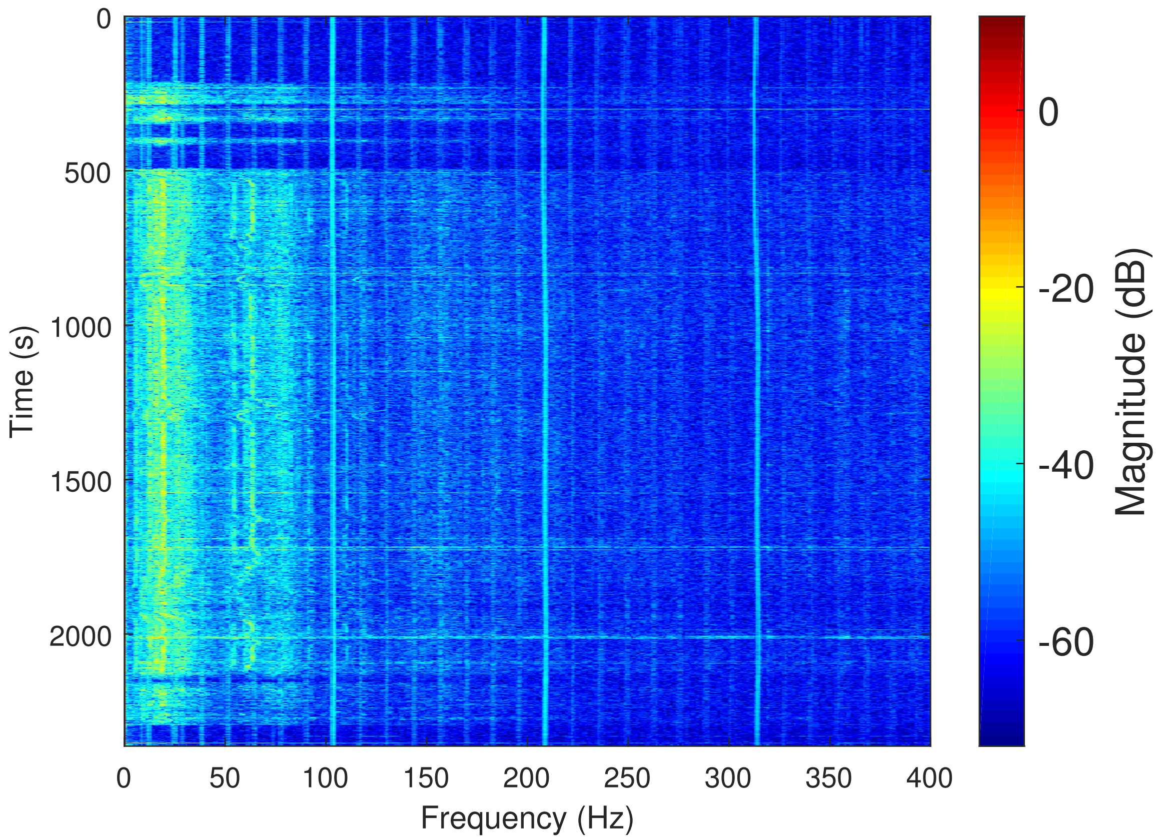

Figure A.3: Waterfall diagram of measurement done on on-road container transport.

B

Minimum mass ratio constraint

During the optimization procedure the ratio of the coupled oscillator harvester, the ratio between the top and bottom mass is varied. To keep the eigenfrequencies of the harvester the same (they should still match the frequencies of the input signal regardless the mass ratio), the stiffnesses should change when varying the mass ratio. For each mass ratio the stiffness is calculated from the relation between the mass and stiffness matrix and the eigenfrequencies of the coupled oscillator:

$$\left|\mathbf{K}-\omega_i^2\mathbf{M}\right| = \left|\begin{bmatrix} k_1+k_2 & -k_2 \\ -k_2 & k_2 \end{bmatrix} - \omega_i^2 \begin{bmatrix} m_1 & 0 \\ 0 & m_2 \end{bmatrix}\right| = 0 \tag{B.1}$$

Calculating the discriminant from eq. (B.1) for both eigenfrequencies gives two equations with k_1 and k_2 as unknowns. These stifnesses are now calculated as

$$k_1 = \frac{m_1(\omega_1^2+\omega_2^2)}{2} \pm \frac{W}{2} \tag{B.2a}$$

$$k_2 = m_2\left(m_1(\omega_1^2+\omega_2^2) \mp \frac{W}{2(m_1+m_2)}\right) \tag{B.2b}$$

with $W = \sqrt{m_1\left(m_1\omega_1^4+m_1\omega_2^4-2m_1\omega_1^2\omega_2^2-4m_2\omega_1^2\omega_2^2\right)}$

which means there are two possible combinations for k_1 and k_2. This is plotted in fig. B.1, where either a combination of stiffnesses form the solid or dashed lines can be chosen. As the expressions for k_1 and k_2 have a root in them, theoretically the stiffness could become complex. As complex stiffnesses have no physical meaning, a constraint can be derived from this formula, i.e. for real k_i, W should not be negative. This yields to

$$m_1\left(m_1\omega_1^4+m_1\omega_2^4-2m_1\omega_1^2\omega_2^2-4m_2\omega_1^2\omega_2^2\right) \geq 0 \tag{B.3}$$

Defining a mass ratio as $R_m = \frac{m_1}{m_1+m_2}$ and the frequency ratio as $R_f = \frac{f2}{f1}$ the maximum possible mass ratio can be expressed in terms of the ratio between the input frequencies:

$$R_m = \frac{4R_f^2}{R_f^4+2R_f^2+1} \tag{B.4}$$

In fig. B.2 the minimum possible mass ratio to avoid (practically impossible) complex stiffnesses is plotted against the eigenfrequency ratio of the coupled oscillator harvester.

This will make it useless to build a coupled oscillator model harvester when the input signal has dominant frequencies that are close to each other. To have a maximum mass ratio of 80%, frequency ratios of 1.6 and less will not be considered in this research.

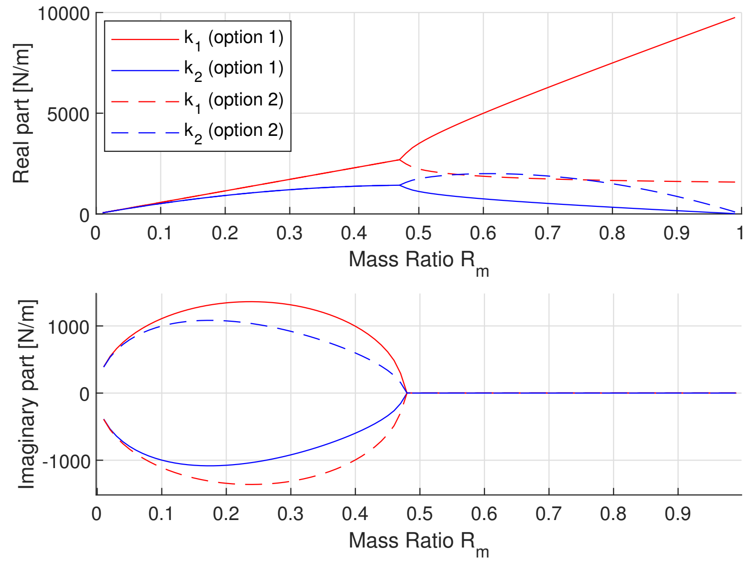

Figure B.1: Plot of the stiffness combinations for a two degree of freedom coupled oscillator as calculated in eq. (B.2). Here the two different stiffness options that can be used to realise eigenfrequencies of 20 and 50 Hz (frequency ratio $R_f = 2.5$) are plotted. When e.g. a mass ratio of 0.7 is preferred, one can either choose to select $k_1 = 6250\ \mathrm{N\,m^{-1}}$ and $k_2 = 520\ \mathrm{N\,m^{-1}}$, or $k_1 = 1740\ \mathrm{N\,m^{-1}}$ and $k_2 = 1880\ \mathrm{N\,m^{-1}}$. The plot clearly shows that the minimum mass ratio is approximately 0.47.

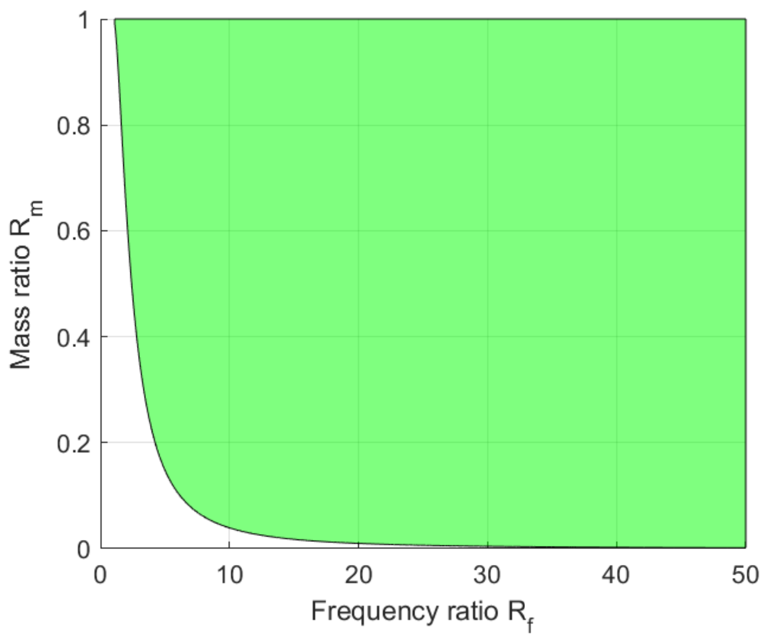

Figure B.2: Possible mass ratios as function of the frequency ratio. The green shaded area represents the mass ratios possible as a function of the frequency ratio. The area is bounded by eq. (B.4) and of course the maximum possible mass ratio of 1.

C

Optimization outcome

In this appendix an overview of the optimization outcome is provided. All optimizations were run for a total mass of $m_t = 0.07$ kg and a parasitic damping of $c_p = 0.014$ as described in part II. As described, the relation $\frac{A_i^2}{f_i}$ is set to $0.05\ \mathrm{m^2\,s^{-3}}$.
Table C.1 shows the case were only a 20 Hz sine wave is used as an input. Shown is the maximum mean power found, together with the optimization parameters that belong to this optimum. Table C.2 shows the case were only a 50 Hz sine wave is used as an input. It becomes clear that the most energy is harvested when the harvester is excited at its first eigenfrequency as described in part II.
In tables C.3 and C.4 the optimization parameters of the two cases described in part II are shown.

Table C.1: Optimizer outcome for coupled oscillator harvesters having eigenfrequencies 20 & 50 Hz. Input signal is a 20 Hz sine wave.

	Coupled oscillator bottom damper	Coupled oscillator top damper	Coupled oscillator both dampers
Mean power (mW)	2.1	2.1	2.1
MR (-)	0.48	0.48	0.48
c_1 ($\mathrm{N\,s\,m^{-1}}$)	1.1	-	0.24
c_2 ($\mathrm{N\,s\,m^{-1}}$)	-	0.14	0.11

Table C.2: Optimizer outcome for coupled oscillator harvesters having eigenfrequencies 20 & 50 Hz. Input signal is a 50 Hz sine wave.

	Coupled oscillator bottom damper	Coupled oscillator top damper	Coupled oscillator both dampers
Mean power (mW)	1.7	0.97	1.9
MR (-)	0.80	0.68	0.80
c_1 ($\mathrm{N\,s\,m^{-1}}$)	0.49	-	0.52
c_2 ($\mathrm{N\,s\,m^{-1}}$)	-	5.0	147

Table C.3: Optimizer outcome for coupled oscillator harvesters having eigenfrequencies 20 & 50 Hz. Input signal is a summation of a 20 & 50 Hz sine wave, i.e. the two tone case from part II.

	Coupled oscillator bottom damper	Coupled oscillator top damper	Coupled oscillator both dampers
Mean power (mW)	2.4	2.1	2.5
MR (-)	0.48	0.48	0.48
c_1 ($\mathrm{N\,s\,m^{-1}}$)	0.93	-	0.32
c_2 ($\mathrm{N\,s\,m^{-1}}$)	-	0.15	0.097

Table C.4: Optimizer outcome for coupled oscillator harvesters having eigenfrequencies 20 & 50 Hz. Input signal is a 20 & 50 Hz sine wave alternately present, i.e. the alternating tone case from part II.

	Coupled oscillator bottom damper	Coupled oscillator top damper	Coupled oscillator both dampers
Applied threshold (mw)	0.8	0.5	1.2
Mean power (mW)	0.88	0.52	1.2
MR (-)	0.58	0.52	0.65
c_1 ($\mathrm{N\,s\,m^{-1}}$)	0.81	-	0.41
c_2 ($\mathrm{N\,s\,m^{-1}}$)	-	1.4	0.083

D

Prototyping

D.1. Calculations

D.1.1. Flexure length calculations

The stiffness of the flexure pair can be calculated by cutting one of the flexures into two, and using Euler-Bernoulli beam theory to calculate the deflection of one of those single sided clamped beams, see fig. D.1.

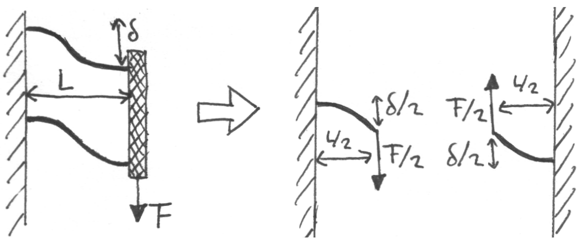

Figure D.1: Calculation method of beam stiffness. As the flexure is prevented from rotating at both ends, the stiffness of one double clamped flexure can be calculated by adding the stiffnesses of two beams that are clamped on one side. The deflection of one half of a single flexure is calculated with Euler-Bernoulli beam theory.

Using Euler-Bernoulli beam theory, we can write that

$$\frac{\delta}{2} = \frac{\left(\frac{F}{2}\right)\left(\frac{L}{2}\right)^3}{3EI} \tag{D.1}$$

with δ the deflection of the mass in m, F the force on the mass in N, L the length of the flexure pair in meter, E the Young's modulus of the flexures in Pa and I the second moment of area in m^4 defined as $I = \frac{wt^3}{12}$ with w and t the width and thickness of the flexure in m assuming a perfect rectangular cross sectional area. Rewriting eq. (D.1) gives the following relation for the stiffness of the flexure pair in $\mathrm{N\,m^{-1}}$:

$$k = \frac{F}{\delta} = \frac{24EI}{L^3} \tag{D.2}$$

D.1.2. Magnetic field calculations

The magnets used in the prototype are grade N50M neodymium (NiFeB) magnets with nickel coating and residual magnetism of $B_r = 1.46$ T [2]. The dimensions of the used magnets are $39.5 \times 13 \times 4$ mm. The magnets are mounted on a stainless steel (AISI 430) back iron with dimensions 45×29 mm with a relative magnetic permeability of $\frac{\mu}{\mu_0} = 2000$ [1].
To calculate the strength of the magnetic flux through the coil wires, the strength of the magnetic field in the spacing between the magnets is simulated in COMSOL Multiphysics [4]. The used coil has a thickness

of 8 mm. The magnets should be further apart than 8 mm as there needs to be some clearance between the moving coil and stationary magnets. The magnetic field has been modelled for clearances of 1 and 2 mm, giving a total distance between the magnets of 10 and 12 mm.

The coil itself is not added to the COMSOL simulation as copper has the same relative permeability as air and thus it will not change the magnetic flux [1]. Figure D.2 shows the magnetic flux density in z-direction around the magnets. Only magnetic field in z-direction matters, as F, B and I should be orthogonal to each other to generate current in the coil wires. The flux density is constant along the x-axis over the span of the magnets.

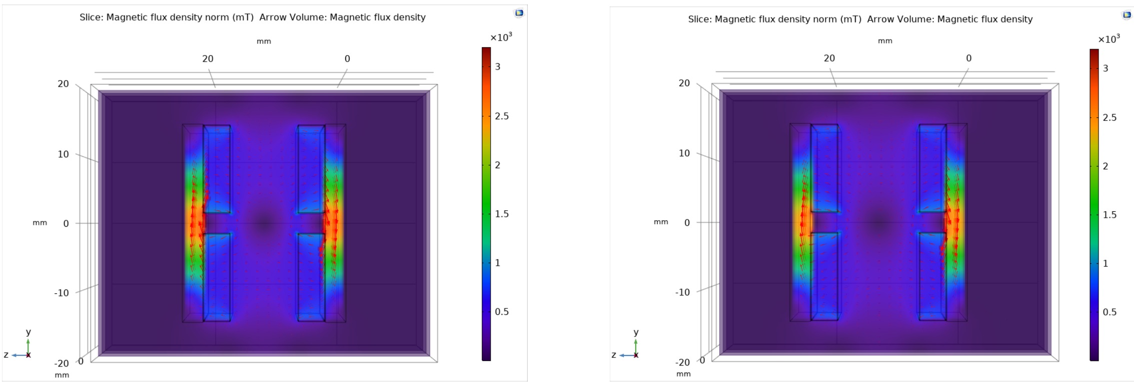

(a) (b)

Figure D.2: Magnitude of magnetic field simulated in COMSOL Multiphysics. Magnets are spaced 12 mm apart.

In figs. D.3 and D.4 the z-component of the magnetic flux is plotted along the y-axis. This is done at $x = 12$ mm (exactly in the middle between the two magnet pairs) and at $x = 16$ mm (at the maximum x-position of the coil). It is visible that the magnetic field at the middle of the coils is weaker than at the sides. Figures D.3 and D.4 also show that placing the magnets further apart decreases the magnetic field strength.

In the prototype, shims of 2 mm were placed between the harvester frame and the magnet holders. This means that the total distance between the magnets is 12 mm.

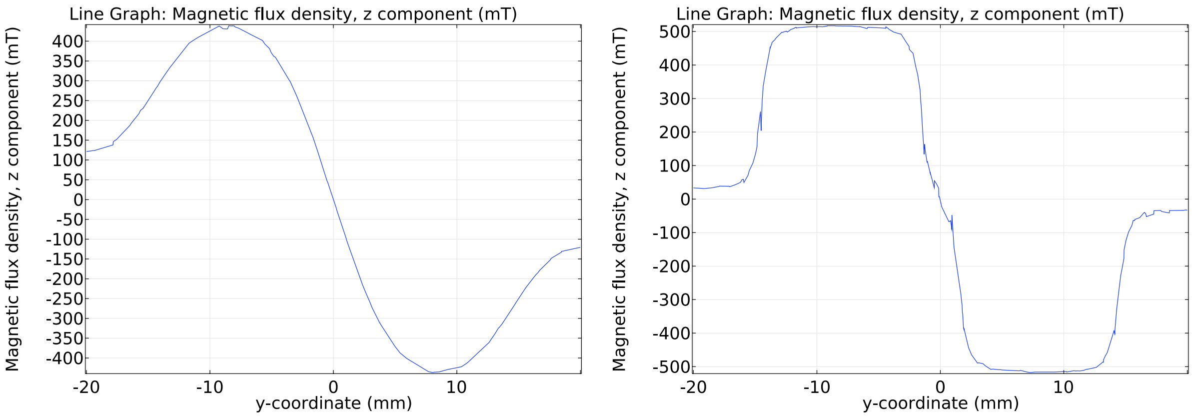

(a) (b)

Figure D.3: Magnetic flux in z-direction (orthogonal to magnetic field and coil motion) plotted along the y-axis for magnets spaced 10 mm apart: (a) in the middle between the two magnet pairs, i.e. at $x = 12$ mm and (b) at the edge of the coil, i.e. at $x = 16$ mm.

The magnetic flux density for the 10 mm spaced magnets as shown in fig. D.3 has been verified by doing measurements on the prototype with a magnetic flux meter. The measurements were performed by manually measuring the magnitude of the magnetic field between the magnet pare using a magnetic field tester (PCE-MFM 3000). This gave a rough idea of the magnetic flux density variation along the y-axis. A maximum magnetic field density of 530 mT was measured, which was constant over a travel distance of more than 8 mm along the y-axis. A high steepness around $y = 0$ (see fig. D.2b) was found experimentally: between the two magnets, the magnetic flux dropped from 500 mT to 12 mT over the range of 2.3 mm along the y-axis.

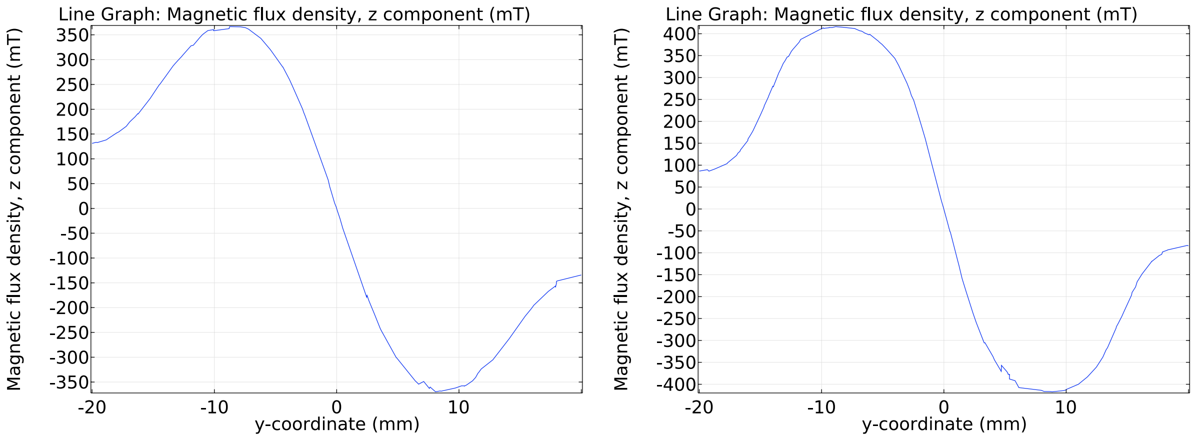

(a) (b)

Figure D.4: Magnetic flux in z-direction (orthogonal to magnetic field and coil motion) plotted along the y-axis for magnets spaced 12 mm apart: (a) in the middle between the two magnet pairs, i.e. at $x = 12$ mm and (b) at the edge of the coil, i.e. at $x = 16$ mm.

D.1.3. Coil impedance calculations

The impedance of the coil is measured to see if this is significant with respect to the coil's resistance. The method described in [3] is used. During the measurement, a shunt resistor of $R_s = 8$ kΩ was used. The source had a frequency of $f = 50$ kHz and a voltage of $V_g = 0.430$ V. The voltage over the coil was measured as $V_x = 0.390$ V, with an phase angle with respect to the source of $\alpha = 65°$. This way a inductance of $L_x = 0.0198$ H was found.
The impedance of the coil can be calculated with

$$Z_L = 2\pi f L_x \tag{D.3}$$

with f the frequency of the AC current through the coil and L the inductance of the coil in H. The maximum coil impedance will be at the highest frequency in the circuit, which will be equal to the highest frequency the oscillator is excited. This is the second eigenfrequency of the coupled oscillator, which is 47.9 Hz. A maximum impedance of 6.2 Ω was found.

D.2. Assembly

Laser cut acrylic sheet was used for structural purposes in the prototype. Thin beams connecting the oscillators with the acrylic reference frame were designed, holding the masses in place until the steel flexures were glued. This way the flexures would have their designed length, and could be glued while relaxed (i.e. unbend). Female pin headers were glued to the oscillating masses. The thin and fragile coil wire was soldered to one end, and thicker wire to the other end. This thicker wire was connected to the data acquisition device.
During assembly, no glue was used to fix the magnets. The fact that the opposing magnets attract each other together with the cut-out slots in the acrylic magnet holders made sure that the magnets were fixed in all three directions. This made disassembly easier as well, as the magnets could be removed one by one at first, before unscrewing the acrylic laser surfaces.

D.3. Experimental testing

D.3.1. Measurement equipment

During experiments, the prototype was mounted on a vibration exciter (shaker) (Brüel Kjær Type 4809). A function generator (BK Precision 4013B) and an external amplifier (Ling Dynamic Systems Ltd. TPO-20) were used to control the shaker. The motion of the ground is measured with both an accelerometer (ADXL335) and laser triangulation sensor ($\mu\epsilon$ ILD1750-2). The oscillating masses are measured with a laser triangulation

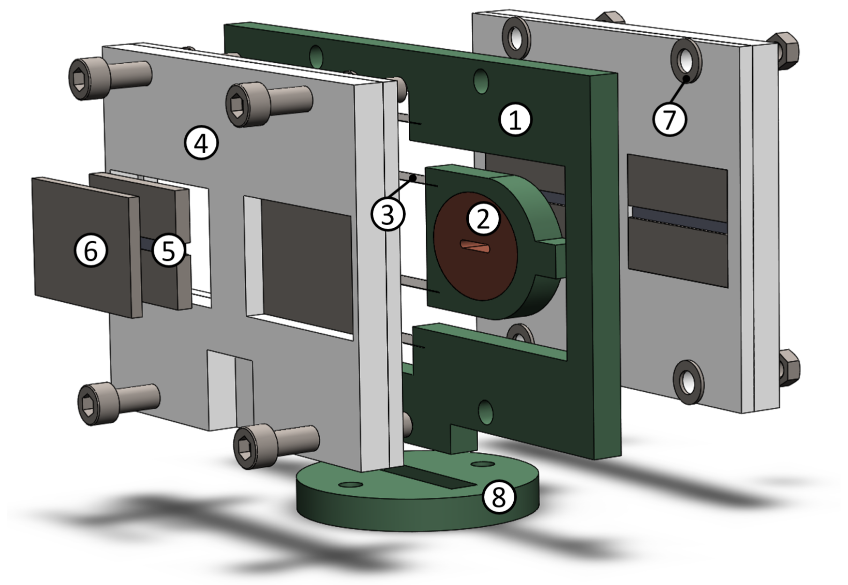

Figure D.5: Exploded view of prototype with ① ground, ② oscillating coil suspended by ③ leaf springs, ④ magne holder with ⑤ magnets and ⑥ back iron. ⑦ Shims were used to create spacing between the oscillating coils and fixed magnets. Bolts with nuts are used to fix the magnet holders to the ground. The ground is glued to a ⑧ mounting plate to fix the prototype to the shaker.

sensor ($\mu\epsilon$ ILD1420-100). Sensors were read out wit a data acquisition box (NI USB6002), sampling at 2000 Hz. A picture of the setup can be found in part II.
During the laser distance measurements isolation tape was added to the surface the laser to prevent scattering of light due to the laser cut acrylic surface which would disturb the measurement.

D.3.2. Presence of higher orders in input signal

During experiments, the vibrations of the ground were at the mounting plate. Figure D.6 shows the FFT spectrum of the measured recordings when exciting the coupled oscillator prototype at 47.9 Hz, which is its second eigenfrequency.

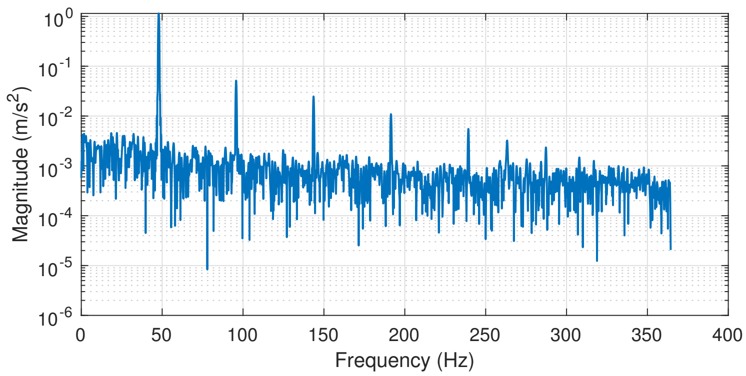

Figure D.6: FFT spectrum of recorded input acceleration when coupled oscillator harvester was mounted on shaker. The prototype was excited at its second eigenfrequency, i.e. 47.9 Hz. Higher order peaks are clearly visible.

D.3.3. Frequency response of prototypes

A frequency sweep has been performed on both the 1DoF and coupled oscillator prototype. No electromagnetic damping was applied to the harvesters during these tests.
In fig. D.7 the response of the 1DoF harvester is plotted for various frequencies. The motion of the shaker

is plotted as well. It is clearly visible that the shaker, having a moving mass and suspension stiffness, adds a degree of freedom to the total system. An anti-resonance peak in the shaker motion occurs close to the harvester's eigenfrequency. The amplification factor, which is the oscillator amplitude divided by the shaker amplitude, is plotted on a third axis.
This frequency sweep was done for both high and low shaker output amplitudes. The difference in amplification factor shows the non-linear behaviour of the steel leaf springs. It can be concluded that this non-linear behaviour is less for lower oscillator amplitudes, as the amplification factor is higher in fig. D.7b.
In fig. D.8 the response of the coupled oscillator harvester is plotted. Again, the anti-resonance peaks in the shaker motion are clearly visible.

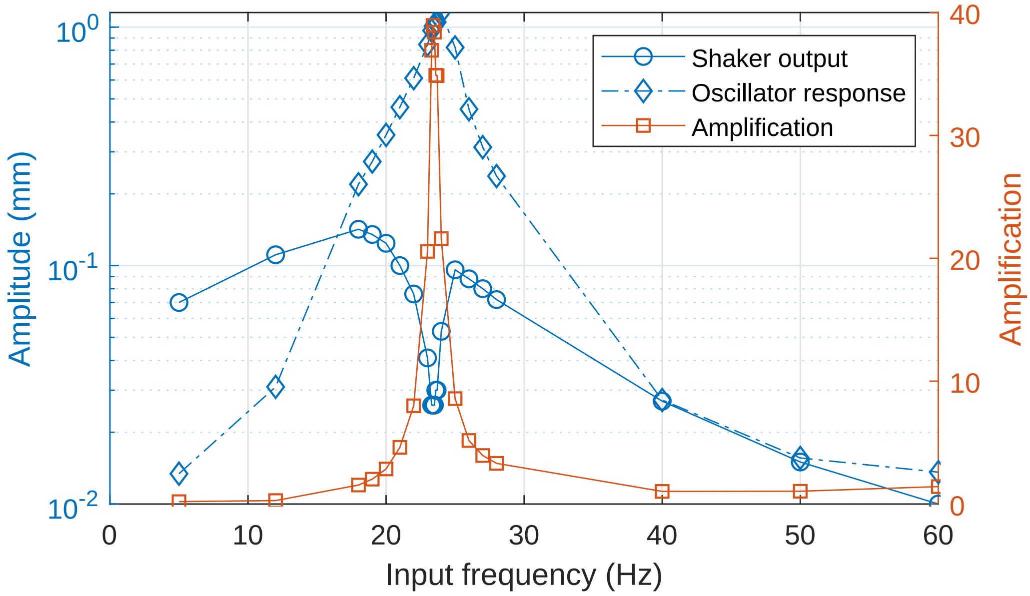

(a)

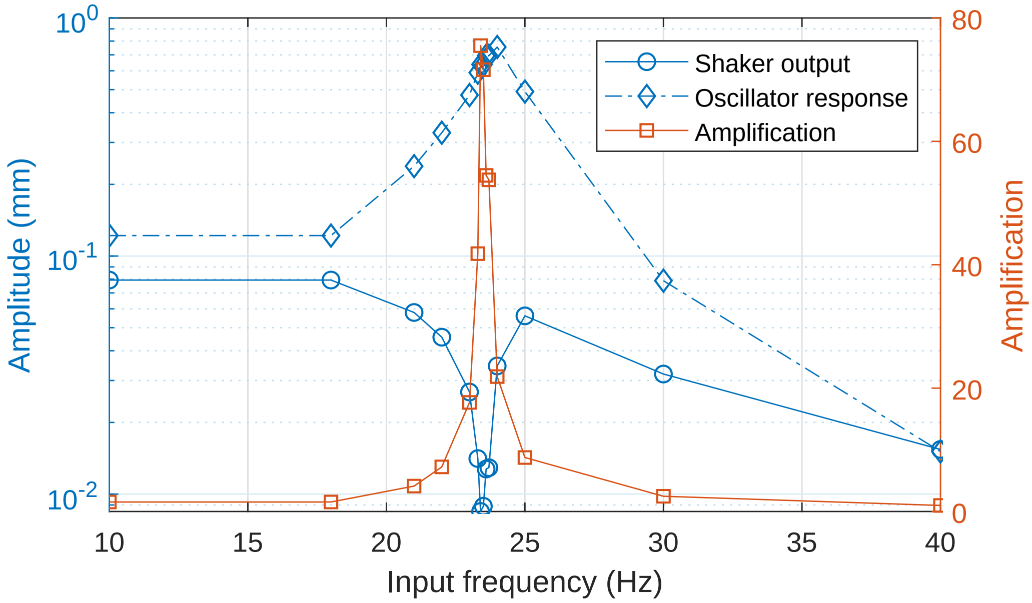

(b)

Figure D.7: System response of single degree of freedom harvester without electromagnetic damping for (a) high input amplitudes and (b) lower input amplitudes for various frequencies.

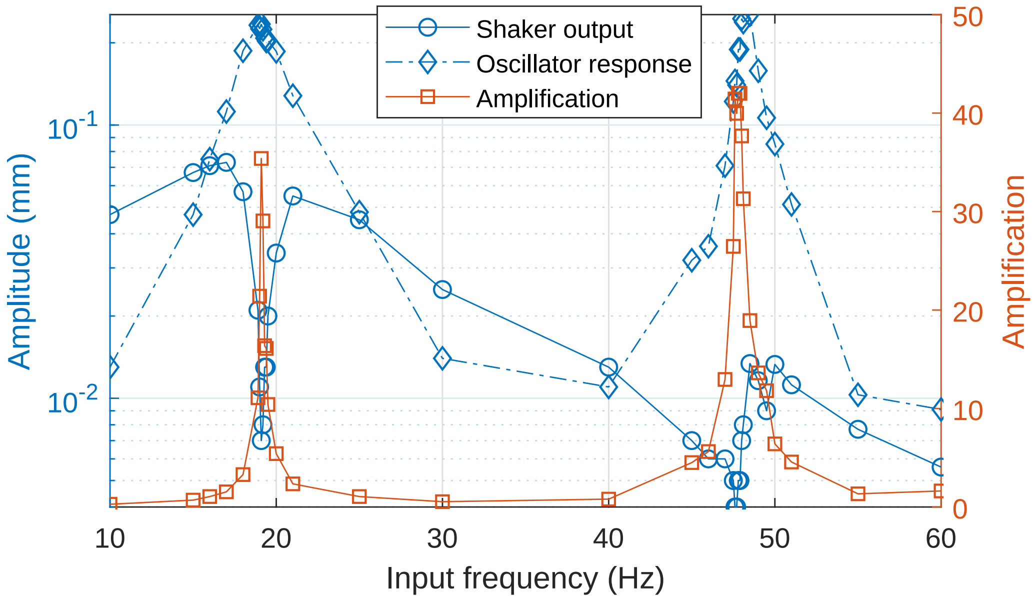

(a)

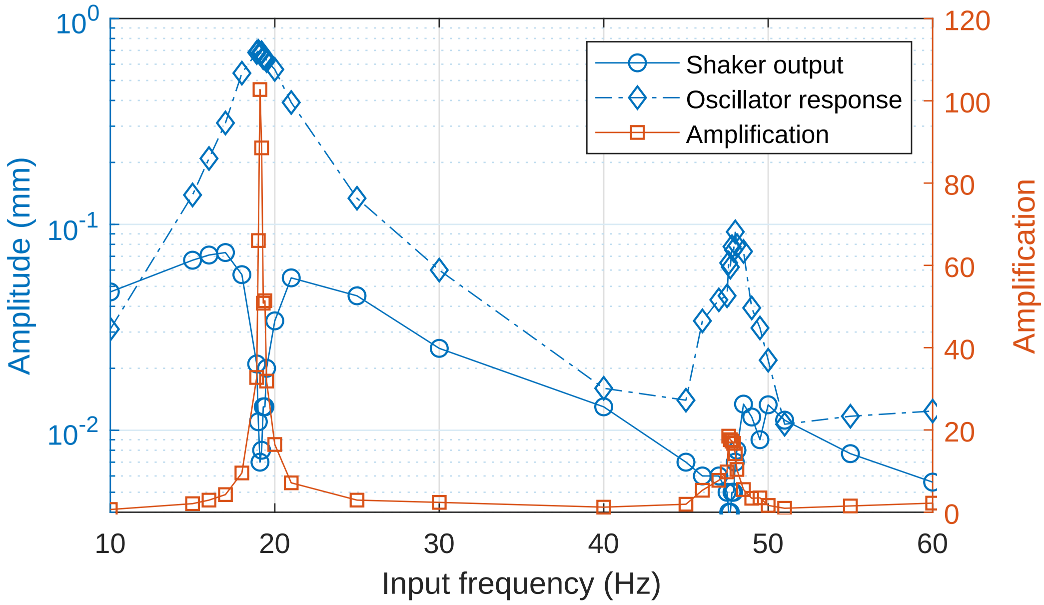

(b)

Figure D.8: System response of coupled oscillator harvester without electromagnetic damping. Plotted are (a) response of the first mass and (b) response of the second mass.

Bibliography

[1] CES EduPack 2018.

[2] Physical magnet data. URL https://www.supermagnete.de/eng/data_table.php. Visited: 08-06-2019.

[3] Freddy Alferink. Measuring self-inductance & esr. URL https://meettechniek.info/passive/inductance.html. Visited: 08-06-2019.

[4] COMSOL Inc. Comsol multiphysics 5.4.